# Luminescence Properties of NaI:Tl and $CeBr_3$ with New Co-dopants

R. W. Sloof

**Cover Text**
possibly
spanning multiple lines

TU Delft

# Luminescence Properties of NaI:Tl and $CeBr_3$ with New Co-dopants

by

R. W. Sloof

to obtain the degree of Master of Science
at the Delft University of Technology,
to be defended publicly on September 28, 2016 at 14:00 PM.

| | | |
|---|---|---|
| Student number: | 1334263 | |
| Project duration: | November 10, 2014 – September 1, 2015 | |
| Thesis committee: | Prof. Dr. ir. P. Dorenbos, | TU Delft, supervisor |
| | Dr.. E. van der Kolk, | TU Delft |
| | Dr.. M. Goorden, | TU Delft |
| | Msc. R. H. P. Awater, | |

*This thesis is confidential and cannot be made public until December 31, 2013.*



TU Delft

# Abstract

The effect of new dopants on the luminescence properties of two types of scintillator crystals have been investigated. First, the luminescence properties of sodium iodine (NaI) crystals doped with thallium (Tl) and co-doped with Sulpher (S) and selenium (Se) were determined. Tl occupies cation sites whereas S and Se are supposed to occupy anion sites in the NaI crystal lattice. Doping with both S and Se led to colouring of the crystals and were not dissolved into the NaI crystal. The light yield and resolution of these crystals were reduced compared with NaI doped with only Tl (NaI:Tl). A fast light intensity decay component was observed for low temperatures (77 – 150 K) when exciting the NaI:Tl crystal with relatively low energy X-rays (<40 keV). This fast component may be responsible for the increase in light yield when going from 150 to 77 K. Next, the luminescence properties of cerium bromide ($CeBr_3$) crystals co-doped with cadmium (Cd), yttrium (Y), lutetium (Lu), and double co-doped with strontium (Sr) and sodium (Na), and strontium (Sr) and calcium (Ca). All co-dopants when dissolved occupy cation sites in the $CeBr_3$ crystal lattice. The $Ce^{3+}$ cations act as a luminescence centre. The $CeBr_3$ with isovalent co-dopants (Y, Lu), showed perturbation of the $Ce^{3+}$ doublet and light traps where this was not expected. The improvement of the light yield at low temperatures is stronger for the CeBr3:Lu crystal compared with that of the undoped and the Y co-doped $CeBr_3$ crystals, suggesting that Lu is better dissolved than Y into the $CeBr_3$ crystal. The divalent co-dopant Cd results in a strong perturbation of the $Ce^{3+}$ doublet and so-called deep traps in the $CeBr_3$ crystal. This causes a weak thermoluminescence intensity as well as low light yield, which strongly improve with decreasing temperature. The double co-doped $CeBr_3$:Sr,Ca crystal showed the strongest perturbation of the $Ce^{3+}$ doublet and highest thermoluminescence below 200 K. This is reflected by the decrease of the light yield in the temperature range of 77 to 200 K. The double co-doped CeBr3:Sr,Na crystal show a weak perturbation of the $Ce^{3+}$ doublet and a weak thermoluminescence due to a low trapping probability for electrons. The $CeBr_3$ crystal with Sr,Ca displays the most proportional behaviour and the highest resolution as well as light yield. The crystal with Sr,Na as co-dopants, on the contrary, has a low resolution and low light yield. The isolvalent co-dopants Y and Lu both showed a moderate proportional behaviour and a low resolution, but Y resulted in a low whereas Lu in a high light yield. The $CeBr_3$ with Lu as co-dopant shows an anomaly at 8 keV in the non-proportionality response curve (proportionality equals 40%). Cd as a co-dopant displayed the lowest light yield and a low resolution, but a reasonable proportionality. The low resolution of all co-dopants except for Sr,Ca were caused by inhomogeneity of the crystals.

# Contents

# 1 Introduction

In this thesis the scintillation properties of two types of inorganic crystals are studied, namely: sodium iodine (NaI) and cerium bromide ($CeBr_3$) with different dopants. A scintillator crystal converts ionizing radiation into light [1]. This phenomenon is used to observe and detect X-rays, electrons, ions, and energetic particles, such as neutrons, photons, and alpha- and beta-particles [2]. The scintillation light of the crystal can be transferred into an electric signal by a photomultiplier tube utilizing the so-called photoelectric effect [2]. The combination of scintillator crystal with a photomultiplier tube makes up a scintillator detector.

The intensity of scintillation light is a measure of the energy of the radiation to which the scintillator crystal is exposed. While the frequency of a specific energy measured is proportional to the intensity of the radiation. The simultaneous recording of the intensity and energy of radiation is called gamma spectroscopy. In gamma spectroscopy a scintillator detector can identify radioactive isotopes, giving important information about the chemical make up of materials and soils. Therefore, scintillator detectors are used in space exploration, for example, to observe the surface of the Moon and Mars. But these detectors are also used on earth for ground exploration to find resources of raw materials and energy (gas and oil) for mining purposes [3]. Scintillator detectors are also used in high-energy physics research to observe elementary particles resulting from high-energy collisions of protons. These experiments are executed, for example, in the Large Hadron Collider (LHC) at CERN in Switzerland [4]. But scintillator detectors are also used in every day life applications, such as: medical imaging and X-ray security. Each of these applications has different standards and priorities for the specification of the scintillator crystals, like: resolution, acquisition time, sensitivity, weight and size, etc. For example, inorganic scintillator crystals as studied here are the best for portable detector tools to discover radioactive isotopes. Therefore, these detectors play a vital role in monitoring compliance with international agreements regarding nuclear material and is instrumental in the disarmament of the worlds nuclear arsenal (nuclear proliferation).

Sodium iodine crystal doped with thallium (NaI:Tl) was the first discovered solid state scintillator in the late 1940s by Robert Hofstadter [5]. The scintillation is caused by the impurities dissolved in the host crystal lattice known as dopants. Other impurities can be added known as co-dopants to further alter the scintillation properties of the crystal. Since the discovery of NaI:Tl as scintillator material many other compounds were discovered.

However, the NaI:Tl crystal is still the most common scintillator crystal used, e.g. as single-photon emission detector for computed tomography in medicine and has been to space in the Apollo 15 to perform gamma spectroscopy of the moon surface [3]. This crystal has good scintillation properties; most prominently of these is the light yield. Also the manufacturing costs of this type of scintillator crystal is low because of the readily available materials needed to make this crystal and the well known and mature technology to produce this crystal. The drawback of the performance of the current NaI:Tl crystals is their non-proportionality response, i.e. a non-linear response of the light yield with respect to the energy of the incoming particle. This also effects the variance of the energy measured due to competing radiative and non-radiative processes. This has a negative effect on the energy resolution of the scintillator, which is important to resolve different components from the recorded spectrum. Hence, the aim of adding new co-dopants to a NaI:Tl crystal is to improve its non-proportionality response and with that its resolution. Earlier attempts of cationic doping showed no improvement on the non-proportionality response [6]. Therefore, the crystals studied in this research have been co-doped with anionic co-dopants, namely: $S^{2-}$ and $Se^{2-}$.

Cerium bromide ($CeBr_3$) scintillator crystals are candidate for future space explorations [7], because they and exhibit a high-energy resolution as well as light yield. Other scintillator crystals that performs slightly better like $LaBr_3$ show intrinsic radioactivity [8]. The Lanthanum in $LaBr_3$ contains a radioactive isotope which will show up in all the measurements. In comparison with sodium iodine scintillator crystal, the cerium bromide crystal performs much better over a large energy range. However, the sodium iodine crystal performs better in the low energy range, its crystal growing techniques are well developed and the resources to create this crystal are much more readily available making sodium iodine a more commercially attractive scintillator. A $CeBr_3$ scintillator crystal also displays good performance at room temperature unlike other high performing scintillator crystals (e.g. germanium, which only performs when cooled by liquid nitrogen which makes it unsuitable for many practical uses.). Since $CeBr_3$ is a relative new scintillator crystal and co-dopants could further improve the scintillator properties makes further investigation of this crystal interesting. Three types of dopants have been studied: (i) isovalent, being yttrium (Y) and lutetium (Lu), (ii) divalent cadmium (Cd) and (iii) double dopants as strontium and sodium (Sr, Na) and strontium and calcium (Sr, Ca). A previous study with a similar scintillator crystal, lanthanum bromide $LaBr_3$, showed promising results when doped with Ce and co-doped with Sr [8]. These dopants yielded an improved proportionality response, energy resolution and makes the crystal mechanically stronger.

This study aims at a better understanding of the effect of co-doping of scintillation crystals on their scintillation properties. This should lead ultimately to improved scintillator crystals tailored for specific applications. Since there is no exact physical model available yet that can predict the changes of scintillation properties by co-doping, experiments are necessary to determine the effects of co-doping on scintillator properties. The NaI:Tl and $CeBr_3$ crystals with the new co-dopants studied in this thesis are expected to improve the scintillation process. The characteristic scintillation properties of these crystals were determined. The light yield was measured in proximity of known radioactive sources by a photomultiplier tube. The decay time was measured by a laser excited X-ray tube at specific temperatures. The luminescence was determined using a high intensity X-ray radiation by a photomultiplier tube with special filters to study the intensity of certain wavelengths of

light and to find the intensity at a specific wavelength as a function of temperature. Due to the hygroscopic nature of the novel NaI and $CeBr_3$ crystals, they were analysed either inside a glovebox or contained in a cryostate under vacuum.

In Chapter 2, the scintillator process is explained and the characteristic properties are considered. In Chapter 3, details of the scintillator crystals studied are given as well as the methods used to determine their properties. In Chapter 4, the results are presented and discussed. Finally, in Chapter 5, the conclusions are summarized and recommendations are given for future research.

# 2

# Theory

In this chapter the physics of the scintillation process will be presented. First, the scintillation process in a crystal exposed to radiation is outlined. For this thesis only $\gamma$- and X-ray interactions are relevant. Next, the effect of elements added to the scintillator crystal, referred to as dopants or co-dopants, will be explained. Finally, the characteristic properties of the scintillator crystals will be discussed. These properties are decay time of the light pulse, non-proportionality and the energy resolution. Also their luminescent spectra and their thermoluminescence are addressed.

## 2.1. Scintillation Process

When incoming radiation hits the scintillator crystal, a flash of light is emitted. Using a photo-multiplier tube and electronics the emitted light is recorded and can be analysed. Before the actual signal is obtained, a series of processes are happening in the crystal. In short, the radiation interacts with the crystal causing ionisation inside of the crystal. The electrons and holes caused by the ionisation migrate towards luminescence centres where it recombines to produce a flash of light. In this study only interaction with photons (both X-rays and $\gamma$-rays) were observed. Therefore only photon interaction is discussed in this report.

### 2.1.1. Interaction of particles with the scintillator

A scintillator material produces a flash of light when it interacts with radiation. The flash contains a number of photons and the exact number is dependent of the energy of the incoming particle [2]. This flash of light can be converted into a pulse of photoelectrons by a photo-cathode, which is part of a photo-multiplying tube (PMT). These photoelectrons are multiplied by the PMT to obtain a stronger signal. When an ionising particle enters the scintillator, it interacts either through Compton scattering or the photoelectric effect. However, when the incoming photon has a very high energy (more than 1 MeV) also pair production can happen. In the sequel these three phenomena are explained.

*Compton scattering*

Compton scattering is inelastic scattering of a particle with an electron of the scintillator material [1]. In this case the incoming particle induces ejection of an electron from the atom. This decreases the energy of the incoming particle equal to the kinetic energy of the emitted electron. A sketch of this interaction is given in Figure 2.1.

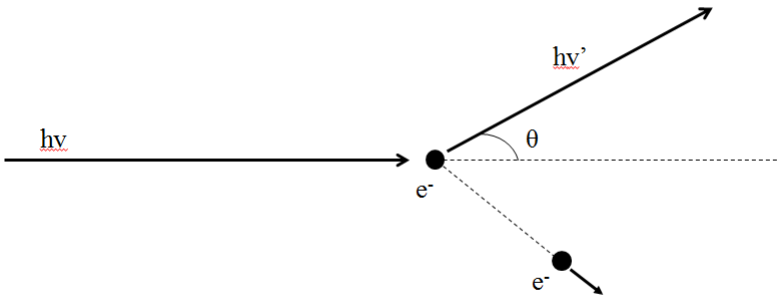


**Figure 2.1:** *Schematic depiction of Compton scattering, where the energy of the incoming electron is hν and the energy of the scattered photon hν' is nonzero, which causes the energy transferred to the scattered electron 'e⁻' to be dependent of the angle θ.*

As shown in Figure 2.1 the incoming e.g. $\gamma$-ray particle has an energy of $h\nu$ and the scattered $\gamma'$-ray particle has an energy of $h\nu'$. The energy of the scattered $\gamma'$-ray particle, assuming that the electron at which it scatters is at rest, is as follows:

$$h\nu' = \frac{h\nu}{1 + \left(h\nu / m_0 c^2\right)(1 - \cos\theta)} \tag{2.1}$$

Where $m_0 c^2$ is the rest mass energy of the electron (511 keV). An expression for the energy lost to the scattered electron can be found:

$$E_C = h\nu - h\nu' = h\nu \left( \frac{\left(h\nu / m_0 c^2\right)(1 - \cos\theta)}{1 + \left(h\nu / m_0 c^2\right)(1 - \cos\theta)} \right) \tag{2.2}$$

Two extreme cases can be identified from Equation (2.2):
1. For $\theta = 0$ the recoil Compton electron has very little energy and the scattered $\gamma$-ray has nearly the same energy as the incident $\gamma$-ray.
2. For $\theta = \pi$ represents a head-on collision. The incident $\gamma$-ray is backscattered towards its direction of origin, whereas the recoil is along the direction of incidence. This extreme represents the maximum energy that can be transferred to an electron in a single Compton interaction.

In normal circumstances, all scattering angles will occur. Therefore a continuum of energies can be transferred to the electron up to the so-called Compton edge, which is the end of the Compton continuum. The gap between the Compton edge and the photo-electron peak equals:

$$E_{C,gap} = h\nu - E_{e-}|_{\theta=\pi} = \frac{h\nu}{1 + 2h\nu / m_0 c^2} \tag{2.3}$$

Inside of the Compton continuum a peak can be found at 250 keV or less. As a result of scattered $\gamma$-particles that had a head-on (or near head-on) collision with an atom-electron. Hence:

$$h\nu'|_{\theta=\pi} = \frac{h\nu}{1+2h\nu/m_0c^2} \tag{2.4}$$

At the limit when the gamma energy is large compared to the rest energy of an electron ($h\nu \gg m_0c^2/2$), Equation (2.4) reduces to:

$$h\nu'|_{\theta=\pi} \cong \frac{m_0c^2}{2} \tag{2.5}$$

The peak corresponding with this energy is denoted as a backscatter peak.

*Photo-electric effect*
Photo-electric effect occurs when the incoming photon transfers all its energy to an electron [2]. This electron is usually a tightly bound core shell electron of the K- or L-shell. The incoming photon must have a higher energy than the binding energy equal to the core level electron. This electron becomes a photo-electron, with a kinetic energy of the energy of the incoming photon minus the binding energy of the core level electron. This electron creates a track of holes and free electrons. The ejection of the electron, which had interacted with an incoming photon, leaves an electron vacancy. This vacancy is filled by one of the outer-shell electron followed by electronic rearrangement and characteristic X-ray emission. Alternatively, the excitation energy of the atom may be transferred directly to one of the outer electrons, causing it to be ejected from the atom [2]. This electron is called an Auger electron and appears with an energy given by the difference between the original atomic excitation energy and the binding energy of the shell the electron was ejected from. In the case of the photo-electric effect, the energy of the incoming photon is wholly absorbed by the scintillator crystal, therefore the resulting measurement is proportional to the energy of the detected radiation. The probability $\tau$ of the photo-electric effect is proportional to the atomic number and inversely proportional to the energy of the incoming particle as in the following equation [2]:

$$\tau \propto \frac{Z^n}{E_\gamma^{3.5}} \tag{2.6}$$

Where $Z$ is the atomic number and $E_\gamma$ is the energy of the incoming photon and the exponential $n$ varies between 3 and 4 depending on the photon energy. The photo-electric effect has a high probability for low values of $E_\gamma$ and for materials with a high atomic number.

*Pair Production*
When the incident photon has an energy largerer than 1022 keV, which is the rest energy of a electron and a positron, the process of pair production is possible [2]. Pair production is not possible with lower energies due to energy conservation. With photons having an energy higher than 1022 keV both an electron and a positron are created in the scintillator crystal. The positron eventually annihilates with an electron emitting a 511 keV gamma ray in the process. Therefore the most noticeable effect of the pair production is the existence of a peak at 511 keV.
Which effect is dominant depends on the atomic number of the scintillating material and the energy of the incoming particle. In Figure 2.2 the dominant effect can be read out for a certain interaction, by intersecting the weighted average Z number of the crystal and the energy of the incoming particle.

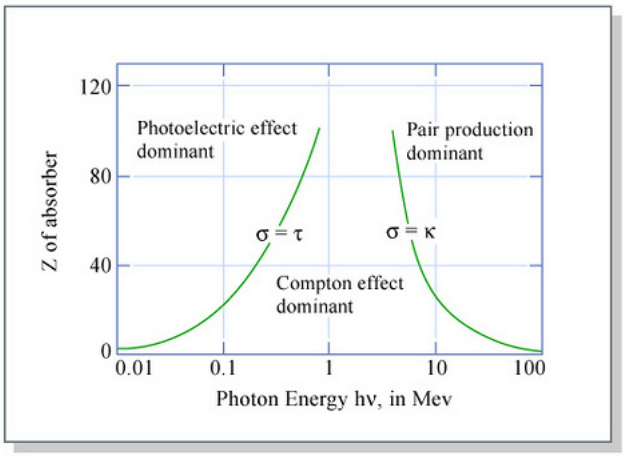


**Figure 2.2:** *Graph showing which effect respectively is dominant after interaction between an incoming particle and a crystal, where $\sigma$ is the probability of a Compton scattering, $\tau$ of the photoelectric effect and $\kappa$ for pair production.*

The photo-electric effect, the Compton scattering and the backscatter peak can be seen from a pulse-height spectrum of Cs-137 shown in Figure 2.3. Cs-137 decays by emitting a $\beta^-$ particle to Ba-137. The Ba-137 nucleus is in an excited state and emits a $\gamma$-ray having an energy of 662 keV when going to its ground state. Since the photon-rays of the Cs-137 isotope do not exceed 1022 keV no pair production was detected.

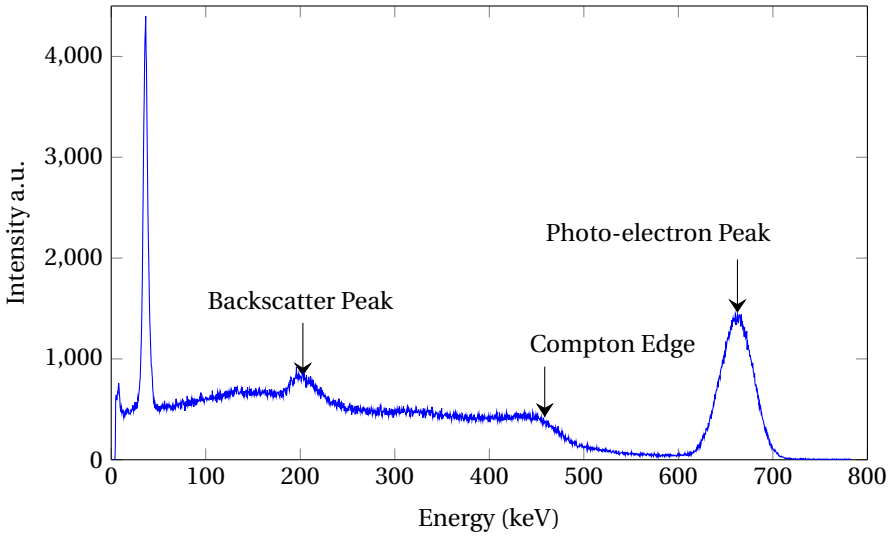


**Figure 2.3:** *Pulse height spectrum of Cs-137 with energy on the horizontal axis and the number of counts or intensity on the vertical axis. A photo-electron peak is visible at 662 keV and the effects of Compton scattering is evident by the Compton edge and the backscatter peak. Taken from [2]*

### 2.1.2. Ionisation

The interactions of the radiation inside the scintillator crystal (see Section 2.1.1) results in the creation of energetic electrons, so-called primary electrons. They pass through the material losing kinetic energy by collisions with other electrons and producing ionisation track(s) of electron-hole pairs, a sketch representing this track is shown in Figure 2.4. The linear ionisation density along the track ($dE/dx$) is inversely proportional to the energy of the primary electron ($dE/dx = 1/E$)[9]. This causes the ionisation density to increase, when the kinetic energy of the primary electron becomes smaller. The electrons and holes diffuse away from the track, the diffusion is effected by the temperature and depends on the mobility of the electrons and holes.

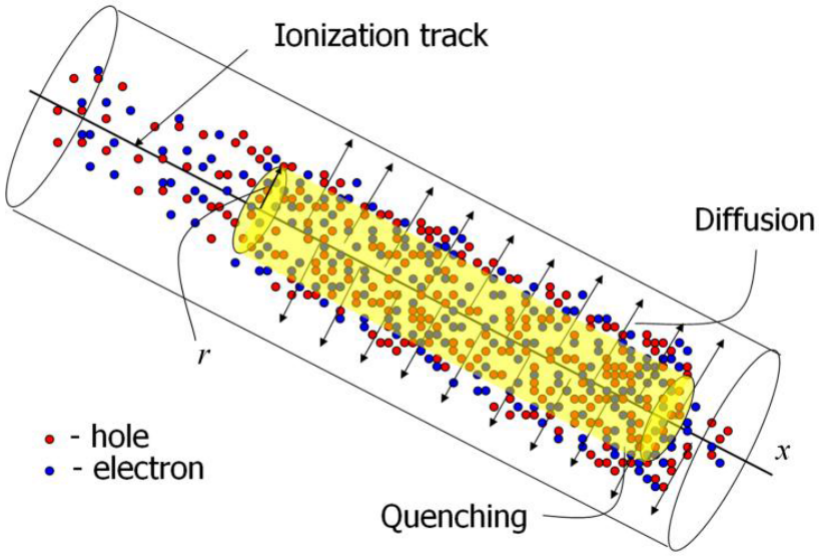


**Figure 2.4:** *: Sketch of an ionization track formed by a primary electron. Starting from the left, free electrons and holes are created which diffuse radially away from the track. Radiation-less carrier recombination occurs at the dense carrier concentration regions. Courtesy of Dr. Khodyuk [10].*

A typical inorganic scintillator material is an insulator with a 4-12 eV gap between the valance band and the conduction band [1]. The primary electron excites a number of electrons (called secondary electrons) to the conduction band leaving holes in the valence band. Both electrons and holes can move freely within the crystal. The idea of a scintillation material is to find an effective way to recombine all the excited electrons in the conduction band with the holes in the valence band via the emission of a photon. The number of photons emitted through this process is a measure for the energy of the incoming particle.

To increase the probability for visible photon emission during the de-excitation process, small amounts of an impurity are added to the inorganic scintillator material. Such deliberately added impurity creates special sites in the lattice at which normal band structure is modified from that of the pure crystal. As a result, there will be energy states present within the forbidden gap through which the electron can de-excite back to the valence band. Since the energy is less than that of the full forbidden gap, this transition can now give rise to a visible photon and therefore serve as the basis of the scintillation process. These de-excitation sites are called luminescence centres [1].

### 2.1.3. Relaxation

After the ionisation, the crystal contains free electrons and holes. The secondary electrons are also energetic and loses their energy through ionisation, creating even more free electrons. This process will stop when all electrons do not have enough energy to eject an atom electron from its valence band. At this point they will lose their remaining energy through collisions until they reach thermal equilibrium. At thermal equilibrium they can recombine at luminescence centres. Typically in a scintillator material the charge carriers will reach thermal equilibrium $k_bT$ within picoseconds. This process is called thermalisation [11]. The charge carriers will diffuse through the crystal until they reach a luminescence centre. At thermal equilibrium the diffusion coefficient $D$ is given by the Einstein equation [9]

$$D = \mu kT \tag{2.7}$$

When the charge carriers reach thermal equilibrium they can recombine at luminescent centres once they reach such a centre. However, the electrons have also other ways of recombination. It is possible that electrons bridge the forbidden gap resulting in lattice emission. This is the primairy source of emission for scintillators like $CeBr_3$. All other recombinations are non-radiative and do not produce light. However, these non-radiative recombinations effect the proportionality between light produced by the scintillator and the energy of the incoming photon. Electron-hole pairs are produced due to the ionisation, such a pair is called an exciton [9]. When two excitons collide, one exciton dissociates non-radiatively and transfers its energy to the other exciton, which dissociates into an electron-hole pair that temporarily has an energy equal to the of the initial energies of both the excitons. However, the excess energy of this electron- hole pair is rapidly lost through a series of transitions that non-radiative transfers its energy to phonons, converting it back into an exciton with the same amount of energy that it had before the collision [9]. Free electrons can also recombine with a hole non-radiatively. These processes quenches the light output of the scintillator and the rate at which this occurs is dependent of the ionisation density ($dE/dx$) and the scintillation material in question. A higher ionisation density has a higher probability for non-radiative interactions. Reducing these non-radiative interactions will improve the proportional response of a scintillator crystal. This can be achieved by co-dopants that create a local electric field which separate electrons and holes. Another quenching process is selfabsorption. This is a phenomenon where the emission of a luminescent centre is re-absorbed by another luminescent centre. This occurs in $CeBr_3$ where the luminescent centre is the $Ce^{3+}$ in the host lattice [12].

### 2.1.4. Non-proportionality response

Since the luminescent and non-radiative processes compete at different rates depending on the ionisation density, a non-linear response to the energy of the incoming particle arises. This non-linear response is denoted as the non-proportionality response of the scintillator crystal. The light yield, which is defined as number of photons per energy of incoming particle, is typically determined at 662 keV. Then, the light yield of the scintillator material irradiated at different energies is taken relative to the light yield determined at 662 keV. This light yield as a function of energy is known as the non-proportionality curve. The non-proportionality yields problems for calibration of a scintillator. Moreover, the non-

proportionality of a scintillator crystal results in a poorer energy resolution (see Section 2.4). An ideal scintillator detector would show no non-proportionality, because then it can be accurately calibrated using one data point since the voltage output is linear proportional to the energy of the measured photon on the whole energy scale. More importantly, the energy resolution would improve without non-proportionality.

### 2.1.5. Recombination and emission

As already mentioned in Section 2.1.2, a typical inorganic scintillator is an insulator with a gap of 4-12 eV between the top of the valence band and the bottom of the conduction band, this is denoted as the forbidden gap [4]. In the valence band all electrons are bound to an atom. When such a valence band electron is excited through radiation it will leave the valence band, provided that the energy of this radiation is larger than the binding energy of this electron. Then the excited electron becomes a free electron in the conduction band, leaving a hole behind in the valence band. As discussed in previous paragraphs, these electrons will continue to create new electrons and holes until they have lost their energy. The electrons and holes do not recombine always efficiently over the band gap, this is the case for a sodium iodine crystal. Hence, impurities are added to the crystal. These impurities must have an energy level inside of the forbidden gap to allow a more effective recombination. The sites at which these impurities are located are called luminescent centres. The luminescent centre therefore introduces energy levels inside of the forbidden gap. Charge carriers can also be trapped. These traps can be deliberately introduced by a co-dopant, shallow traps can still migrate to luminescent centres and can effectively improve the light yield. However, at lower temperatures such a trap releases its charge carrier much slower and a deep trap releases its charge carrier slower even at high temperatures.

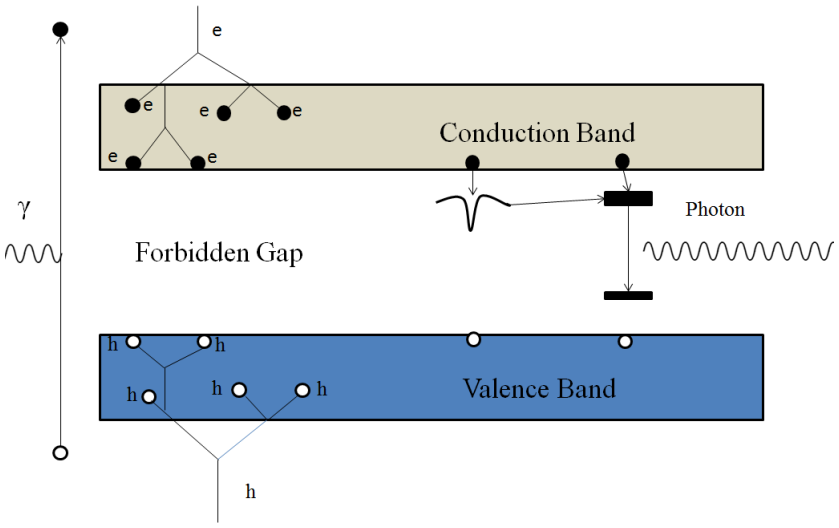


**Figure 2.5:** *A schematic representation of the scintillator process. From left to right: Interaction, relaxation, trapping of electrons and recombination, after [4]*

For NaI:Tl the recombination process is as follows [1]:

$$\begin{aligned} Tl^{+} + h &\rightarrow Tl^{2+}, \qquad Tl^{2+} + e \rightarrow h\nu \\ Tl^{+} + e &\rightarrow Tl^{0}, \qquad Tl^{0} + h \rightarrow h\nu \end{aligned} \tag{2.8}$$

Equation (2.8) shows the recombination of either a electron or a hole with the luminescent centre $Tl^+$. The ground state of the electron configuration of $6sTl^+$ is ${}^1S_0$ and the lowest excited state states of the 6s6p configuration are: ${}^3P_0$, ${}^3P_0$, ${}^3P_2$ and ${}^3P_1$ [1].
The emission spectrum of NaI:Tl is strongest between 300 and 550 nm, with a peak at 420 nm. This emission is related to ${}^3P_1 \rightarrow {}^1S_0$ transitions of $Tl^+$ ions. Since the PMT is sensitive between 200 and 600 nm [13], the emission of NaI:Tl is optimal for a scintillator detector.

The $CeBr_3$ crystal can recombine efficiently through the host lattice with an emission of a photon. For $CeBr_3$ the recombination of the $Ce^{3+}$ involves to a 5d → 4f transition. $Ce^{3+}$ has a single electron in the 4f shell [14]. The spin-orbit coupling causes a splitting into a ${}^2f_{5/2}$ ground state and ${}^2f_{7/2}$ state. This transition causes an emission in $CeBr_3$ centered at 361 and 390 nm at 78 K [12] and is denoted as a $Ce^{3+}$ doublet; see Figure 2.6. The recombination process of $CeBr_3$. This doublet can be perturbed by $Br^-$ vancancies. These vacancies can be deliberately introduced by divalent co-dopants, which cause vacancies due to charge compensation.

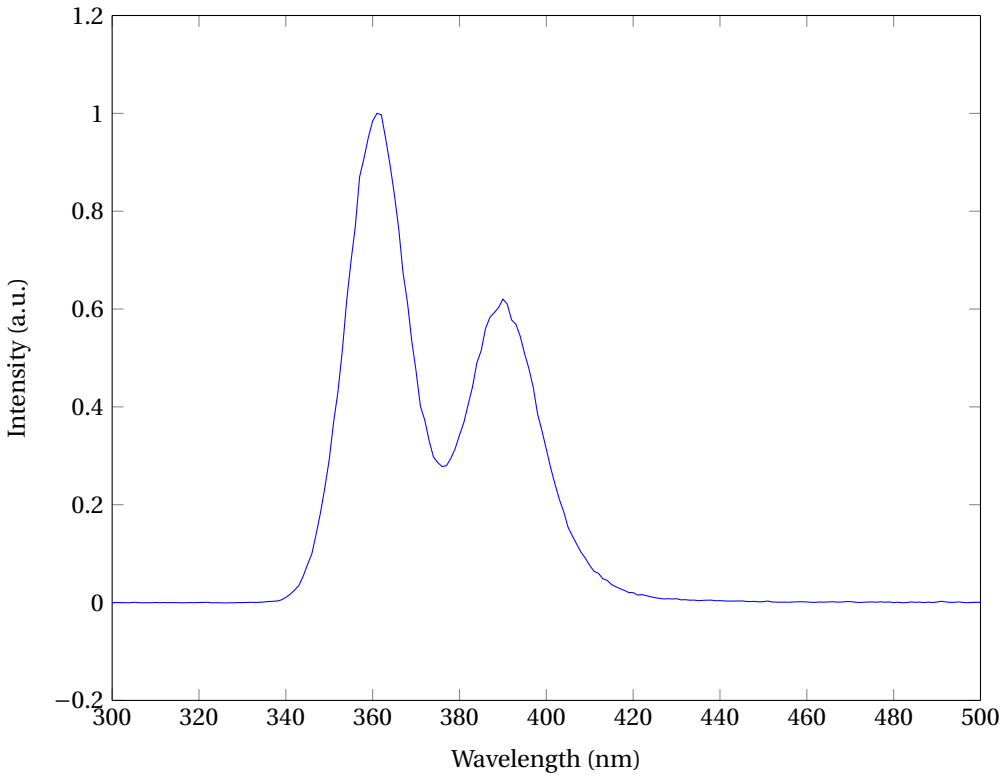


**Figure 2.6:** *Emission spectrum undoped $CeBr_3$.*

The interaction of electrons, holes and excitons with phonons can bring localisation of the valance hole in a regular lattice, known as self-trapping [12]. After thermalisation a hole reaches the top of the valence band and localises at a distinct anion. The ion transforms into an atom $X^- \rightarrow X^0$. The state $X^0$ polarises the environment and the system exhibits an axial relaxation resulting in sharing the hole between neighbouring anions. This is known as a $V_k$ centre. This $V_k$ centre can recombine with an electron and the resulting luminescence is called the intrinsic luminescence [1]. When the emission of the intrinsic luminescence overlaps the emission of the luminsecent centre self-absorption occurs. As the light

is re-emitted in the case of self-absorption no light loss occurs. However, the selfabsorption increases the decay time constant (i.e. the elapsed time when half of the emissions occurs), this is undesirable as the decay time constant is ideally as short as possible (see Section 2.3). This effect was found in $CeBr_3$ [12]. The self-absorption chance of $CeBr_3$ could be decreased by introducing co-dopants which alter the emission spectrum of $CeBr_3$.

## 2.2. Structure and properties of co-doped scintillator crystals

Inorganic scintillators are often doped with elements that becomes a luminescence centre in the crystal. An inorganic scintillator can, however, also be doped with elements that do not result in luminesce [1]. These elements are co-dopants and often decrease the light yield of the scintillator. But these co-dopnat are added to improve other properties of the crystal. For instance, $LaBr_3$ and $CeBr_3$ both have a hexagonal lattice and are therefore brittle [15]. This is undesirable for practical use as cracks in the crystal decreases its light yield and results in lower ingot yields [16]. To improve the mechanical properties $LaBr_3$ was co-doped by $Sr^{2+}$. Tests of the performance of this LaBr3 scintillator crystal showed a more proportional response [8].

### 2.2.1. Crystal structure NaI:Tl and $CeBr_3$

NaI has a cubic rock salt crystal structure in which the ionic radii of $Na^+$ and I are 102 and 220 pm [17], respectively; see Figure 2.7. Since the iodine anion is much larger than the sodium cation, the dimensions of the crystal lattice are determined by the iodine anions.

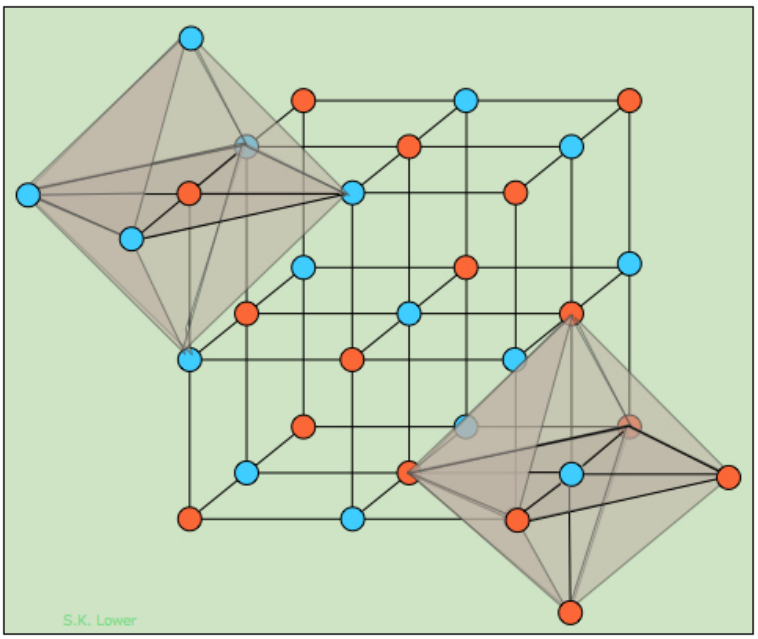


**Figure 2.7:** *Depiction of the crystalline structure of a NaI crystal.*

$CeBr_3$ has a hexagonal crystal structure; see Figure 2.8. As in the NaI crystal, the Br-anion has a much larger ionic radius than the $Ce^{3+}$ cation, 196 versus 101 pm. The coordination number of $Ce^{3+}$ in this structure is 6 [17]. All co-dopants replaces the $Ce^{3+}$ inside the hexagonal crystal structure.

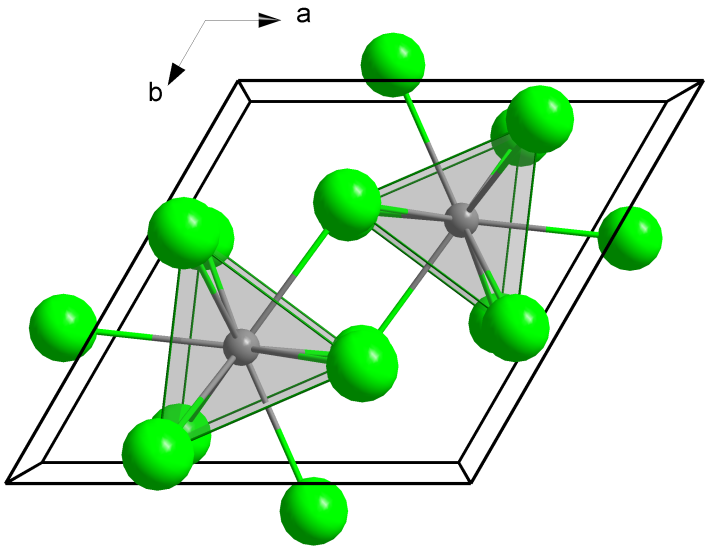


**Figure 2.8:** *Depiction of the crystalline structure of a $CeBr_3$ crystal. Where grey stands for $Ce^{3+}$ and green for Br−.*

### 2.2.2. Effect of co-dopants on mechanical and scintillator properties

For the application of a scintillator crystal in a detector it must be robust. When cracks occur inside the crystal it will impair its integrity. Moreover, such cracks cause the light inside of the crystal to scatter and therefore cracks decreases the light yield of a scintillator. The strength of a scintillator crystal can be enhanced by adding co-dopants [15]. These co-dopants increases the critical resolved shear stress by forming obstacles for movement of dislocations [18].

For example, in order to strengthen the hexagonal structured $LaBr_3$ it was co-doped with $Sr^{2+}$ and $Ba^{2+}$ [19]. These co-dopants not only improved the critical resolved shear stress, but also improved the light yield, energy resolution and proportionality. The exact mechanism of how the co-dopants improve these characteristics is yet not fully understood. These co-dopants have a different valence than $La^{3+}$, therefore it will create vacancies, due to charge compensation, inside of the crystal structure. These vacancies can trap electrons, because the local charge is higher. If these traps are shallow enough at room temperature the electron can escape this trap through its thermal energy. At higher ionisation densities a non-radiative de-excitation of the electron is more likely. Thus a trapped electron that leaves the trap is more likely to de-excitate radiatively.

## 2.3. Decay time constant scintillator

The decay time constant gives an indication of the duration of the crystals emission. The decay time constant is defined as the elapsed time where half of the emissions takes place. This is an important property of the crystal as it causes an afterglow in the crystal, where another interaction takes place inside the crystal before the previous reaction is resolved. Therefore, the decay time constant indicates a maximum amount of activity it can reliably measure. The intensity of the light pulse decays exponentially with time according to:

$$I(t) = I_{max} e^{\frac{-t}{\tau_d}} \tag{2.9}$$

Where $I$ is the intensity, $I_{max}$ is the maximum intensity and $\tau_d$ is the decay time constant of the scintillator material.

The time response of a scintillator material depends both on the transport of electrons to luminescent centres and the lifetime of those luminescent centres. The transport to the luminescent centres is discussed in the ionisation and relaxation section; 2.1.2 and 2.1.3 respectively. The lifetime of the luminescent centres is determined by their transition rates between the excited state and the ground state. The radiative lifetime (i.e. the transport of electrons to luminescent centres and the lifetime of those luminescent centres) $\tau$ is defined by [14]:

$$\Gamma = \frac{1}{\tau_d} \sim \frac{n\left(n^2+2\right)^2}{\lambda^3} \left|\left\langle f \middle| \mu \middle| i \right\rangle\right|^2 \tag{2.10}$$

Where $\lambda$ is the emission wavelength, $n$ is the refractive index and $\left\langle f \middle| \mu \middle| i \right\rangle$ is the matrix element connecting the initial and final state of the transition via the electric dipole $\mu$. For $CeBr_3$ the radiative lifetime forms the major contribution to the decay time, whereas for NaI:Tl the transport to the luminescence centres is more prevalent. This is due to the fact that $CeBr_3$ luminescence through the host lattice and NaI:Tl through the Tl co-dopants. $CeBr_3$ therefore has a short decay time constant of around 17 ns at room temperature, the radiative lifetime of luminescent centres can be substantial. However, as is the case of $Eu^{2+}$ which is in the order of 350-400 ns [4].
The decay time determines the maximum activity a scintillator is able to reliably measure, because a second radiation hits the scintillator crystal before the first one is resolved the scintillator gives an output of one measurement with an energy of the first plus the second. The decay time also gives an indication of the effect of a co-dopant. When many shallow traps are present, for instance, the decay time is increased.

## 2.4. Resolution

When an incoming particle has a well defined energy the output signal of a scintillator detector shows a Gaussian distribution; see Appendix A1. The resolution of a scintillator is defined as the full width at half maximum divided by the energy of the peak location; see Figure 2.9. This resolution is determined by three contributions: the intrinsic resolution of the scintillator $R_{int}$, transport resolution $R_{tr}$, and the resolution of the detector $R_M$. The intrinsic resolution of the scintillator crystal depends on two parts: the non-proportionality response $R_{npr}$ and the inhomogeneity of the crystal $R_{inh}$. Therefore, the formula for the resolution is:

$$\left(\frac{\Delta E}{E}\right)^2 = R_{npr}^2 + R_{inh}^2 + R_M^2 + R_{tr}^2 \tag{2.11}$$

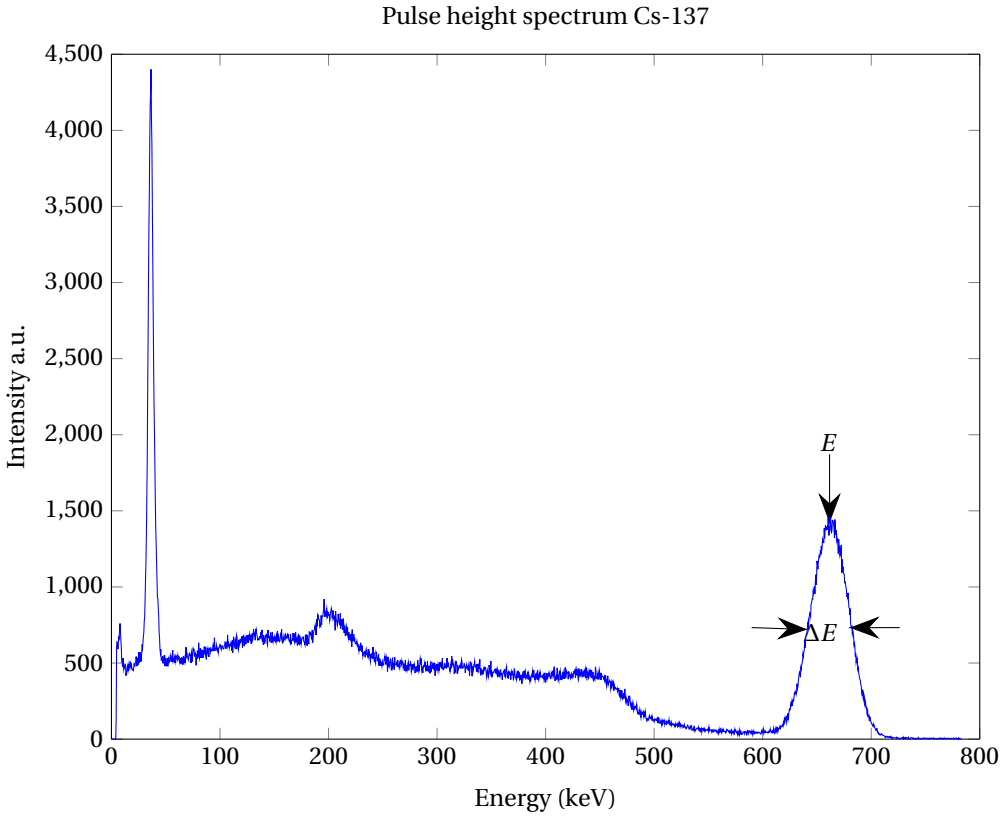


**Figure 2.9:** *Pulse height measurement of Cs-137 where the energy (E) of the photo-electron peak is defined at the top of the Gaussian distribution and the full width at half maximum of this peak (ΔE) are pointed out.*

The resolution of the scintillator is an important property of a scintillator, as it defines how much detail can be detected in a spectrum. Photons with a small difference in energy end up inside the same Gaussian peak due to a too low resolution where it is hard to distinct them from one another. Also the narrower the Gaussian peak the less acquisitions are necessary to to obtain a well-defined peak. This shortens the acquisition time for any experiment.

The increase in resolution due to the non-proportionality response is related to the competition between the gain and loss processes of the interactions; see Section 2.1.4. The loss and gain processes that occurs for each event differ. This causes the peak to broaden. The higher the non-proportionality the greater the difference between loss and gain processes of each event. This results in a poorer resolution.

The resolution contribution of the inhomogeneity, non-proportionality and the transport are dependent of the specific properties of a scintillator crystal. The contribution of the PMT depends on of the light yield of the crystal and variance of the PMT, according to:

$$\left(\frac{\Delta E}{E}\right) = \sqrt{2}\ln(2)\sqrt{\frac{1-\nu(M)}{N_{phe}^{PMT}(T)}} \tag{2.12}$$

Where $\Delta E$ is the full width half maximum of the peak, $\nu(M)$ is the variance of the single electron peak and $N_{phe}^{PMT}(T)$ is the light yield at the position of the peak. The factor $\sqrt{2}\ln(2)$

is applied because it goes from variance to full width half maximum. Equation (2.12) dictates that the resolution will be better for higher energies, because then more photoelectrons are produced by the scintillator.

# 3

# Materials and Methods

First, details on the composition and dimensions of the sodium iodine and cerium bromide scintillator crystals with different dopants as used in this study will be presented. Next, the methods and equipment used to determine the properties of these scintillator crystals will be addressed. The equipment used for recording of scintillator crystals light yield as a function of the excitation energy at room temperature (luminecence) will be explained. The same equipment is used for measuring this light at a fixed energy but as a function of temperatures. Next, the measurements of pulseheight spectra of the light generated with different $\gamma$- and X-ray sources are described. Finally, the measurements of the time dependent decay of the light after X-ray excitation are explained.

## 3.1. Materials: The Scintillator Crystals

### 3.1.1. Sodium iodine scintillator crystals

Two commercial sodium iodine crystals doped with thallium (NaI:Tl) encased with aluminium were supplied by Saint-Gobain (France); see 3.1. These crystals having a diameter and height both of 25.4 mm. Henceforth, the two crystals are denoted as A and B.

**(a)** *Crystal A.* **(b)** *Crystal B*

**Figure 3.1:** *Two commercial NaI:Tl crystals from Saint-Gobain used to study their non-proportionality response.*

Three other bare, i.e. without aluminium casing, sodium iodine crystals were also investigated. One crystal coped with thallium (NaI:Tl) was grown at Saint-Gobain (France). The two other crystals co-doped with sulphur (NaI:Tl,S) and with selenium (NaI:Tl,Se) were grown at University of Bern (Switzerland). These crystals were grown by the vertical Bridgeman technique inside a sealed quartz ampoule and in 8 mm ingot. Next, the crystal were

cleaved along a (001) plane with a volume of 30-40 $mm^3$. All dopants and co-dopants are supposed to make up 0.5 wt% (added to the melt) of the crystal. The $Tl^+$ dopant replaces a $Na^+$ ion inside the crystal lattice. The $S^{2-}$ and $Se^{2-}$ replaces $I^-$ ion inside the crystal lattice causing vacancies to occur, due to the difference in valency. The crystals are shown in Figure 3.2.

**Figure 3.2:** *Photo taken of the NaI doped and co-doped crystals. From left to right: NaI:Tl; NaI:Tl,S and NaI:Tl,Se.*

The size of the crystals investigated are reported in Table 3.1.

**Table 3.1:** *Dimensions of the doped and co-doped NaI crystals.*

| Crystal | Length (mm) | Width (mm) | Height (mm) |
|---|---|---|---|
| NaI:Tl | 9.6 | 8 | 3.1 |
| NaI:Tl,S | 4 | 4 | 3 |
| NaI:Tl,Se | 4 | 4 | 4 |

Note that due to the irregular shape of the crystals this is only an indication of their sizes.

### 3.1.2. Cerium bromide scintillator crystals

All co-doped $CeBr_3$ crystals were produced at University of Bern by the vertical Bridgman technique in sealed quartz ampoules and in 8 mm diameter ingots, then cleaved into 30-50 $mm^3$ fragments and are suppose to contain 0.5 wt% of each co-dopant. The co-dopants can be split up into 3 groups: divalent co-dopant $Cd^{2+}$ , isovalent co-dopant $Y^{3+}$ and $Lu^{3+}$, and double dopants $Sr^{2+}$,$Ca^{2+}$ and $Sr^{2+}$,$Na^+$. All dopants replaces $Ce^{3+}$ inside the hexagonal $CeBr_3$ crystal lattice. The crystals studied were photographed and shown in Figure 3.3.

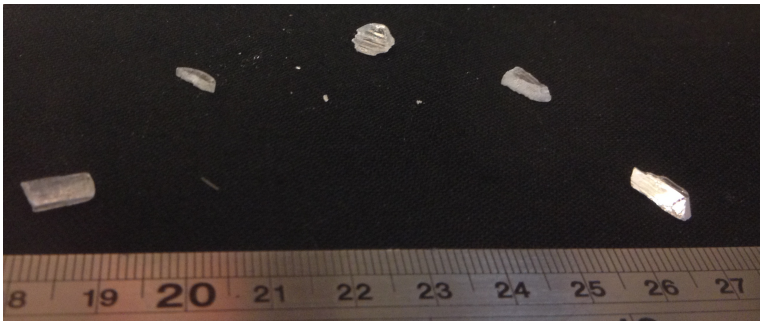

**Figure 3.3:** *Photo taken of the co-doped $CeBr_3$ crystals studied. From left to right: $CeBr_3$ crystals co-doped with, Y, Cd, Lu; Sr,Ca and Sr,Na, respectively.*

The crystals were all clear but have various sizes. The sizes at the time of the measurements are reported in Table 3.2.

**Table 3.2:** *Dimensions of the co-doped $CeBr_3$ crystals.*

| Crystal | Length (mm) | Width (mm) | Height (mm) |
|---|---|---|---|
| $CeBr_3$:Cd | 7 | 3.8 | 2 |
| $CeBr_3$:Y | 12 | 4 | 3 |
| $CeBr_3$:Lu | 10 | 4 | 1.3 |
| $CeBr_3$:Sr,Na | 9.5 | 6.5 | 3 |
| $CeBr_3$:Sr,Ca | 12 | 4.4 | 2 |

Note that due to the irregular shape of the crystals this is only an indication of their sizes.

## 3.2. X-ray Excited Luminescence and Thermoluminescence

Figure 3.4 displays the set up used to obtain the X-ray excited photoluminescence and thermoluminescence spectra. The luminescence spectra were obtained using a X-ray tube with Cu anode operated at 60 kV and 25 mA. The samples examined were kept in place with a needle spring making thermal contact with the cold finger of a Janis VPF-800 cryostat. The emission of the samples was focused via a quartz window and a lens on the entrance slit of an ARC VM504 monochromator (blazed at 300 nm, 1200 grooves/mm dispersed) and recorded with a Hamamatsu R943-02 PMT. Both the cryostat and the monochromator were operated under vacuum. The emission spectra were corrected for the monochromator transmission and the quantum efficiency of the PMT. X-ray excited luminescence measurements were performed at liquid nitrogen temperature (i.e. at 77 K). The PMT was mounted outside the cryostat and remained always at room temperature.
The thermoluminescence spectra were taken by observing the intensity of the peak position of the luminescence obtained at liquid nitrogen temperature. After X-ray irradiation of typically 20 minutes the X-ray beam was turned off. After switching off the X-ray beam the crystals under study were heated by a LakeShore 331 temperature controller at a rate of 6 K/min. The thermoluminescence was measured at 450 nm for the NaI:Tl samples and at 388 nm for the $CeBr_3$ samples, except for $CeBr_3$:Sr,Na which was observed at 361 nm.

## 3.3. Pulse-height measurements

The resolution, light yield and the non-proportionality were determined with pulse height measurements. These measurement were performed at room temperature with a standard Bialkali Hamamatsu R1791 PMT for the resolution and the non-proportionality response and a super Bialkali Hamamatsu R6231-100 PMT was used to determine the light yield connected to a Cremat CR-112 and an Ortec 672 spectroscopic amplifier with 0.5-10 µs shaping time. The signal is forwarded to a single channel analyser, which assigns the pulse to a channel depending on their height. For all pulse-height measurement a shaping time of 10 µs was used. The spectra were rebinned to 8 channels in one bin. The crystals were mounted on the window of the PMT and then covered with an umbrella of teflon. This method was used to reflect all light towards the PMT [20]. Due to the hygroscopic nature of the NaI and $CeBr_3$ crystals, all pulse-height measurements were performed inside a M-Braun dry glove box with a moisture level of less than 1 part per million. The light yield was obtained by comparing the position of the peak position of the 662 keV photoelectron peak with the position of the mean value of the single electron spectrum. The single electron spectrum is the spectrum of the PMT without any light. Due to the voltage single electrons

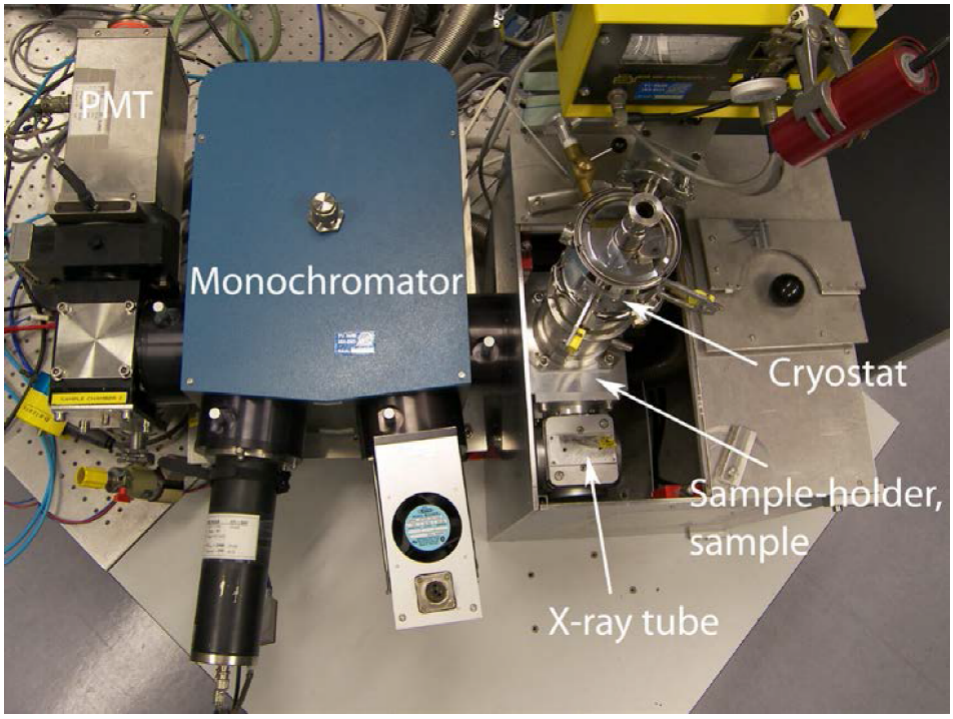


**Figure 3.4:** *Experimental set up for X-ray excited luminesence and thermoluminescence, courtesy of Dr. Alekhin.*

may leak through resulting in a signal. The peak and its properties were determined as described in Appendix A2.

### 3.3.1. Photomultiplier Tube

The photomultiplier tube (PMT) is used to multiply the amount of electrons that is generated by its photocathode into a measurable electric charge. The amount of electrons emitted by the photocathode depends on the amount of incident photons. Incident photons are the photons scintillated by the crystal. The amount of incident photons depends on the energy of the gamma radiation that enters the crystal and the quantum efficiency of the photocathode. The quantum efficiency is simply:

$$QE = \frac{number\ of\ photoelectrons\ emitted}{number\ of\ incident\ photons} \tag{3.1}$$

Equation (3.1) gives the efficiency by which the photocathode converts photons to photoelectrons and is sensitive for wavelengths between 200 to 600 nm [21]. This ideally would be at 100% but in practice never is. The efficiency is a property of the specific photomultiplier tube used.

The basic principle of the photomultiplier tube is that the photoelectrons emitted by the photo- cathode are multiplied by a series of dynodes [2]. When a photoelectron hits a dynode, it is multiplied through secondary emission as shown in Figure 3.5. The principal of secondary emission is that an electron hitting a dynode generates electrons that are emitted. This is achieved by accelerating the incident electrons with an electrical field. This electrical field is created by applying a voltage between the dynodes, the photocathode and the anode.

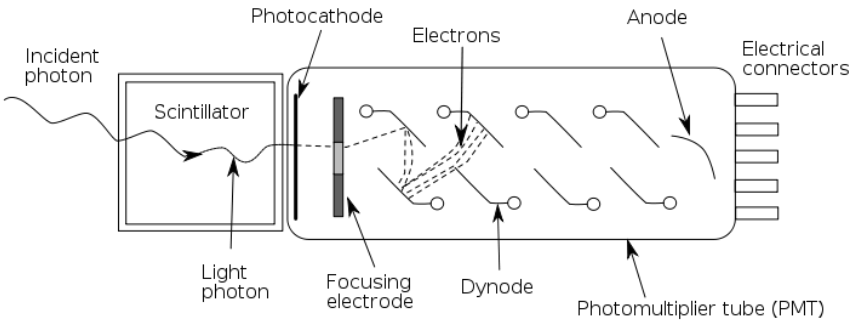


**Figure 3.5:** *Schematic depiction of a scintillator detector.*

Since every dynode multiplies the number of electrons the total amount of electrons increases exponentially with an overall gain of:

$$overallgain \sim \delta^N \tag{3.2}$$

Where $N$ is the number of dynodes and $\delta$ is the number of photoelectrons released per dynode. The primary purpose of a photomultiplier tube is to amplify the number of the photoelectrons created by the crystal and the photo-cathode. But there are also a few unwanted effects. One of them is the spontaneous photo-electron emissions. It is possible that a photo-electron is emitted without an incident photon from the crystal. The photomultiplier tube will dutifully increase the gain of this photo-electron and a measurement is made without an actual radiation event. Because this occurs with a single photo-electron, it is possible to use this phenomenon to determine how much a single electron is amplified. With this information it is possible to determine how many photoelectrons were present before applying the gain. Therefore the light yield can be determined quantitatively.

### 3.3.2. Radioactive sources

A Cs-137 with 0.5 MBq activity and an Am-241 with 0.5 MBq activity were placed in proximity of the samples to obtain their pulse-height spectra. Also a variable X-ray source was applied. This variable X-ray source contains an Am-241 source that emits 60 keV $\gamma$-rays producing $K_\alpha$ and $K_\beta$ X-rays from Cu, Rb, Mo, Ag, Ba and Tb targets. A high activity (30 MBq) Cs-137 source was used for temperature dependent light yield measurements. This source was encased in stainless steel absorbing most of the 32 keV X-rays.

### 3.3.3. Temperature dependent light yield measurement

Pulse height spectra were also taken outside of the glovebox with a Janis VPF-800 cryostat. The crystals examined were pressed by a needle spring inside a cup, covered with aluminium foil, facing the PMT to ensure that the maximum amount of light was reflected towards the PMT. This PMT was mounted on the cryostat with a berrylium window in between the sample. Perpendicular to the PMT a highly active Cs-137 source was placed. It is assumed that the light yield at room temperature is the same of that at 300 K. Therefore the peak position of the 662 keV peak, and with that the relative light yield relative to the light yield at room temperature, at temperatures ranging from 77 to 500 K was determined relative to the peak position at 300 K.

## 3.4. Time resolved measurement of an optical signal

The light intensity of the scintillator crystals were established with a time correlated single photon counting. The measurements were performed with a pico second X-ray tube at temperatures ranging from 77 to 500 K. This tube excites the crystal by shooting X-rays at the sample. The X-rays are controlled by a picoquant Sepia multichannel laser diode, which shoots light pulses at a set frequency to the photocathode of the X-ray tube. Every time the laser light hits the photocathode X-rays are emitted. A single photon detector is placed perpendicular to the direction of the X-rays facing the crystal, detecting the moment the crystal starts scintillating. This process is schematically visualised in Figure 3.6. The moment the laser sends out a pulse is used as a start signal and the detection by the single photon detector is used as a stop signal. The sample is inside a Janis VPF-800 cryostate under vacuum. A time to analogue converter analyses the time between the start and stop signal. An electronic counter records the number of a certain time registered by the set-up. This results after many start/stop cycles into a time resolved evolution of the light intensity, which is schematically depicted in Figure 3.7.

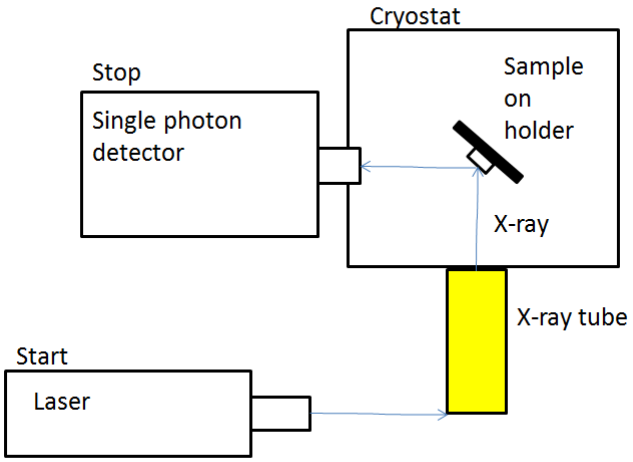


**Figure 3.6:** *Schematic representation of the picosecond X-ray set up.*

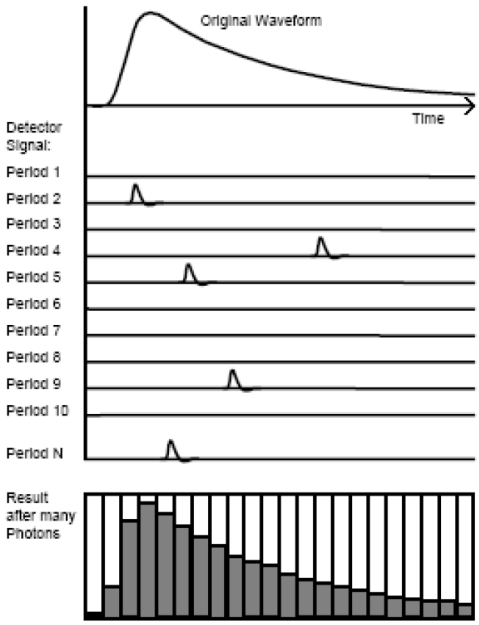


**Figure 3.7:** *Representation of the process of constructing the time resolved light pulse using the start/stop cycles.*

During experimentations a LakeShore 331 temperature controller was used to set the temperatures of the crystals at 77, 100, 150, 200, 250 300, 400 and 500 K. When the cold finger of the cryostat reached the set temperature a waiting period of 15 minutes was taken to ensure that the crystal would be at the same temperature. The laser frequency was set to allow enough time to pass between excitation to ensure that two decay processes would not overlap. This frequency was limited to 170 kHz in order to not overstress the X-ray tube. For the co-doped $CeBr_3$ crystals the laser frequency was set to 170 kHz and a time scale of 0.5 µs was chosen. The settings for NaI:Tl and NaI:Tl,S crystals are summarised in Table 3.3.

**Table 3.3:** *Settings of the pico second X-ray set up for NaI:Tl and NaI:Tl,S.*

| Temperature (K) | Frequency laser (kHz) | Time scale ($\mu$s) |
|---|---|---|
| 77 | 60 | 20 |
| 100 | 60 | 20 |
| 150 | 60 | 20 |
| 200 | 60 | 20 |
| 250 | 60 | 10 |
| 300 | 60 | 10 |
| 400 | 180 | 2 |
| 500 | 180 | 2 |

# 4

# Results and Discussion

Sodium iodine (NaI) and cerium bromide ($CeBr_3$) crystals with different co-dopants (cf. Section 3.1) are investigated to study their effect on the scintillation properties. First, the incorporation of the co-dopants into the crystal lattice of the scintillator crystals is considered. Next, the X-ray excited luminescence spectra of the crystals recorded at liquid nitrogen temperature are presented and discussed together with the luminescence when excited with X-rays as function of temperature (thermoluminescence). Thereafter, the non-proportionality, resolution and light yield of the crystals are compared with each other. Then, the X-ray excited light pulse evolutions and the determined decay constants are given and evaluated. Finally, the results of the temperature dependant light yield measurements are addressed.

## 4.1. Co-doped Scintillator Crystals

Sodium iodine (NaI) and cerium bromide ($CeBr_3$) inorganic of scintillator crystals with different dopants are investigated (cf. Section 3.1).

Sodium iodine crystal doped with thallium (NaI:Tl) is commercially available and serves as a reference; cf. Section 3.1.1. The ionic radius of $Na^+$ is 102 pm which is much smaller than that of $Tl^+$, i.e. 150 pm [17]. However, the $Na^+$ ions occupy the octahedral site of the I sublattice of which the ionic radius is much larger (220 pm). This octahedral site is estimated from the lattice parameter of NaI (647 pm) and amounts 207 pm. Thus Tl can replace Na in the crystal, since $Tl^+$ fits easily in the NaI host lattice.

The anionic co-dopants $S^{2-}$ and $Se^{2-}$ replaces $I^-$ in the NaI scintillator crystal. Due to charge neutrality, this is associated with a vacancy in the Na sub-lattice. The ionic radii of these co-dopants (184 and 198 pm [17], respectively) are smaller than the ionic radius of $I^-$ (220 pm) and thus fit in the NaI host lattice.

However, in Figure 3.2 it is shown that NaI:Tl,Se has a dark colour. This suggests that the co-dopant $Se^{2-}$ did not dissolve into the NaI:Tl crystal. No pulse height spectra could be measured from this crystal. The dark colour suggests that this is due to too much absorption of light and therefore no meaningful results were found for this crystal.
The NaI:Tl,S looks clear, but on closer examination some black spots can be found. This suggests that the Sulphur did not completely dissolve into the crystal lattice.

The cerium bromide crystals were co-doped with divalent $Cd^{2+}$, isovalent co-dopant

$Y^{3+}$ and $Lu^{3+}$ , and double dopants $Sr^{2+}$,$Ca^{2+}$ and $Sr^{2+}$, $Na^{+}$; cf Section 3.1.2. In case of the divalent $Cd^{2+}$ vacancies are created at the $Br^{-}$ sub-lattice to obey charge neutrality. One vacancy is expected per co-dopant site. In case of the double divalent co-dopants it is expected that they also create vacancies at the $Br^{-}$ sub-lattice. The divalent and single valent double co-dopant Sr,Na are also expected to create vacancies at the $Br^{-}$ sub-lattice. The single valent Na dopant is expected to create two vacancies to obey charge neutrality. It is possible that the divalent and single valent are next to one another inside the crystal. In this case a site with three vacancies can occur.

All co-dopants replaces the $Ce^{3+}$ inside the hexagonal crystal structure of $CeBr_3$; see Figure 2.8. The coordination number of $Ce^{3+}$ in this structure is 6 and its ionic radius equals 101 pm [17]. The ionic radii of the co-dopants are tabulated, see Table 4.1. The ionic radius of $Na^{+}$ is practically the same as that of $Ce^{3+}$.

**Table 4.1:** *Ionic radius of the $Ce^{3+}$ and the co-dopants [17].*

| Cadion | Ionic radius (pm) |
|---|---|
| $Ce^{3+}$ | 101 |
| $Y^{3+}$ | 90 |
| $Lu^{3+}$ | 86 |
| $Cd^{2+}$ | 95 |
| $Sr^{2+}$ | 118 |
| $Ca^{2+}$ | 100 |
| $Na^{+}$ | 102 |

The ionic radius of $Sr^{2+}$ is larger than that of $Ce^{3+}$ (118 versus 101 pm), however, as in the NaI crystal, the anion $Br^{-}$ has a larger ionic radius than the cadion $Ce^{3+}$ (196 versus 101 pm), which enhances the space for cations like $Sr^{2+}$, but not enough to fit easily on cation sites in the $CeBr_3$ crystal lattice.

The $Na^{+}$, $Ca^{2+}$ and $Sr^{2+}$ already showed improvement on proportionality and resolution as single dopants [22]. Therefore these dopants are known to dissolve into the crystal.

## 4.2. Luminescence and thermoluminescence spectra

### 4.2.1. NaI:Tl and NaI:Tl,S Crystals

The X-ray excited luminescence spectra of the NaI:Tl and NaI:Tl,S crystals shown in Figure 4.1 appear almost identical with maximum at 426 nm. Thus the emission is not affected by the sulphur co-dopant. It is expected that this co-dopant does not form a luminesence centre (see Section 2.1.5), however, the presence of the co-dopant could cause a shift in the emission spectrum and this was not observed. As such this emission spectrum suggests that the co-dopant is not homogeneously distributed inside the crystal.

The thermoluminescence was determined at the maximum of 426 nm.

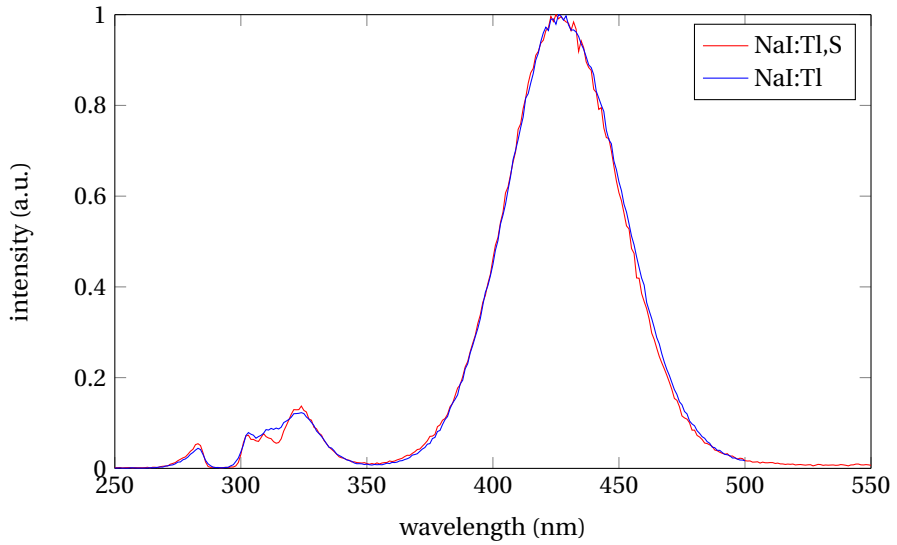


**Figure 4.1:** *Photoluminescence excitation spectra of NaI:Tl and NaI:Tl,S crystals recorded at 77 K.*

The fact that there are no real differences in the shape of the photoluminescence suggests that the $S^{2-}$ ions were not in proximity of the luminescence centres. Also no emission from sulphur occurs in the range 250 to 550 nm. Given that the PMT is sensitive for wavelengths from 300 to 600 nm, it is unlikely that sulphur contributes to the light yield.

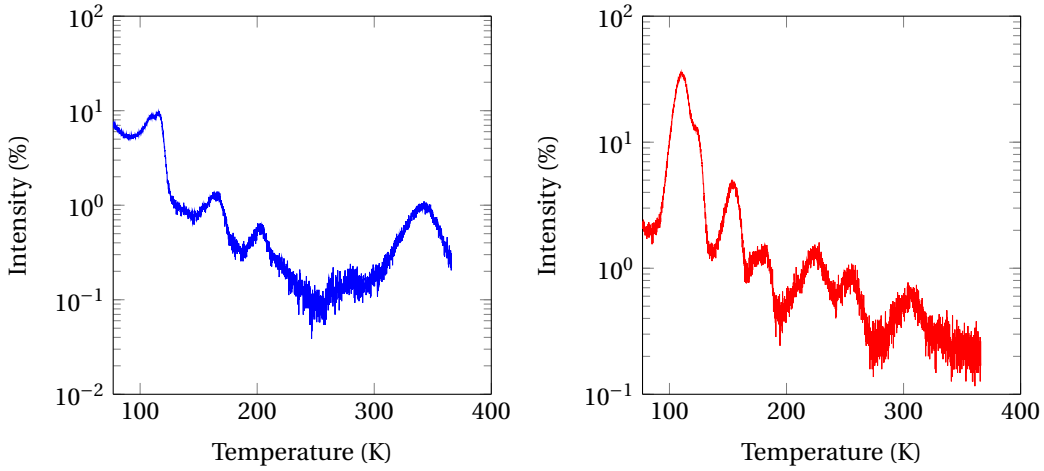


**Figure 4.2:** *Thermoluminescence glow curves of NaI:Tl (left) and NaI:Tl,S (right). The curves are normalised to the steady state X-ray excited luminescence intensities at 426 nm.*

The thermoluminescence of NaI:Tl,S shows two more peaks than NaI:Tl and the intensity of the thermoluminescence of NaI:Tl,S is overall higher below 280 K, see Figure 4.2. The thermoluminescence below 200 K is associated with shallow traps. This is associated with small defects in the crystal. The peak at 300 K shown in both NaI:Tl and NaITl,S can be attributed to the thallium doping, as these peak are of the same order of magnitude. The two peaks between 200 and 300 K is seen only in the NaI:Tl,S thermoluminescence spectrum and is caused by the sulphur doping.

### 4.2.2. Co-doped $CeBr_3$ crystals

The luminescence spectra and the thermoluminescence of the $CeBr_3$ co-doped crystals are presented in Figure 4.3. All the luminescence spectra show signs of a perturbed $Ce^{3+}$ doublet. This perturbation could be caused by the presence of the aliovalent co-dopants (Cd, Sr , Ca and Na), which causes vacancies to occur inside the crystal, see Section 2.1.5. For isovalent co-dopants (Y, Lu) no perturbation of the $Ce^{3+}$ doublet is expected. This indicates that the perturbations observed in the luminescence spectrum for Y and Lu was caused by vacancies due to imperfections in the crystal. $CeBr_3$:Y shows more thermoluminescent activity than $CeBr_3$:Lu. The resolution of $CeBr_3$:Y is also higher than that of $CeBr_3$:Lu. This indicates that the $CeBr_3$:Y contains more vacancies than $CeBr_3$:Lu.
For the divalent co-dopants a perturbation is expected due to vacancies, which are present to obey charge neutrality; see Section 2.1.5. In the case of Cd and Sr, Na the thermoluminescence is weak at maximum just above 1 %, for Sr, Na a second luminescent peak is showing at 200 K. This is probably due to the single valent Na co-dopant as it is expected that it creates deeper traps than the divalent co-dopants. The low thermoluminescence of $CeBr_3$:Cd crystal is peculiar as traps are expected due to the perturbation of the $Ce^{3+}$ doublet. This could indicate that the traps caused by the Cd sites do not release at room temperature and are so-called deep traps; see Section 2.2.2. Co-doping with Sr,Ca shows a strong perturbed $Ce^{3+}$ doublet and a strong thermoluminescence (10 %), because of the low resolution (see Table 4.4) of Sr,Ca these traps can be attributed to the presence of the co-dopants.

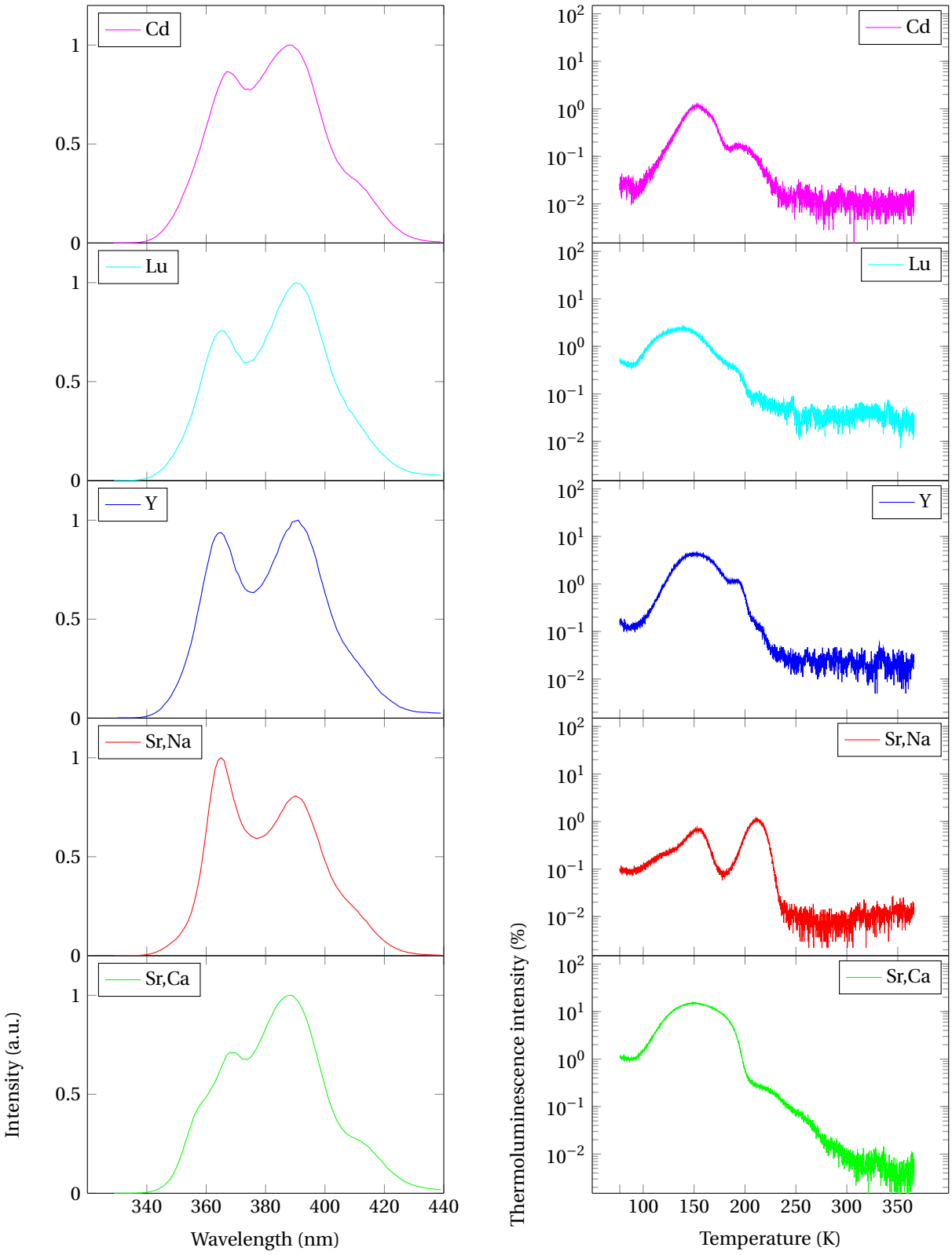


**Figure 4.3:** *Photoluminescence of $CeBr_3$:Cd, $CeBr_3$:Lu, $CeBr_3$:Y, $CeBr_3$:Sr, Na and $CeBr_3$:Sr,Ca crystals at 77 K and thermoluminescence glow curves of the same crystals. The curves are normalised to the steady state X-ray excited luminescence intensities at 388 nm, except for the $CeBr_3$:Sr,Na crystal which is at 361 nm.*

## 4.3. Non-proportionality, resolution and light yield

### 4.3.1. Encased NaI:Tl

The non-proportionality of two aluminium encased NaI:Tl crystals (denoted A and B, respectively) was determined at room temperature. To this end, pulse height spectra were recorded using the following radioactive sources: Cs-137 (662 keV), Am-238 (60, 33, 26 keV), Ba X-rays (32 keV); cf. Section 3.3.2.

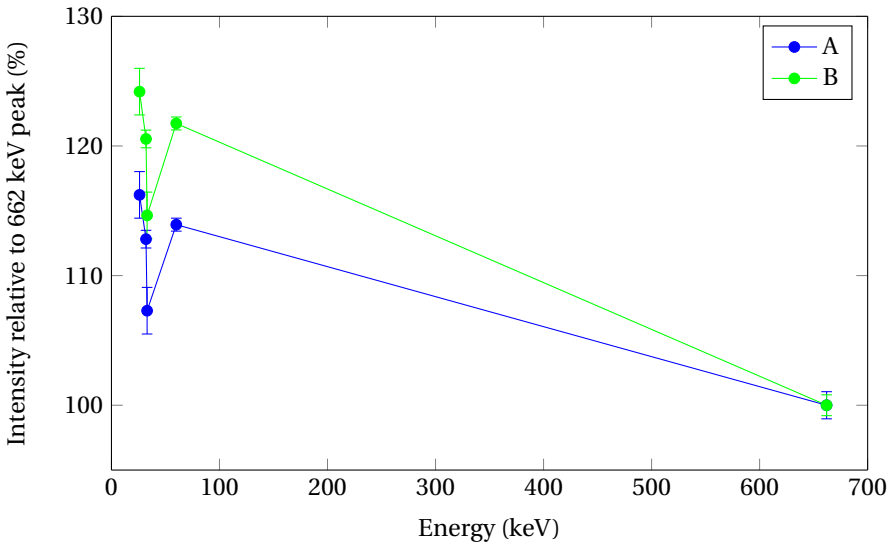


**Figure 4.4:** *Non-proportionality response relative to the 662 keV peak of encased NaI:Tl crystals A and B at room temperature.*

The non-proportionality curve of these two crystals have a similar shape, but crystal A has a more proportional response. This implies that the non-proportionality of NaI:Tl can differ from one another, even though they were manufactured around the same time at the same factory; see Section 3.1.1.

The resolution of both crystals, see Table 4.2, has been determined from the same recorded pulse height spectra as used to determine their non-proportionality response.

**Table 4.2:** *Resolution of encased NaI:Tl crystals*

| Crystal | Resolution (%) |
|---|---|
| A | $6.1 \pm 0.1$ |
| B | $6.1 \pm 0.1$ |

Although the two crystals differ in their non-proportionality response, their resolution is the same within the experimental error. This is due to other contributions to the energy resolution, i.e. the contribution of the PMT, transition and inhomogeneity.

### 4.3.2. Bare NaI:Tl and NaI:Tl,S crystals

Pulse height spectra were taken with a Cs-137, an Am-241 and a variable X-ray source in proximity of the NaI:Tl,S and NaI:Tl crystals. From these spectra the relative non-proportionality was determined, as shown Figure 4.5. The NaI:Tl,S shows a very similar non-proportionality response as the NaI:Tl crystal. The uncertainty of the data points is much larger for the NaI:Tl,S than NaI:Tl due to a much higher resolution, see Table 4.3.

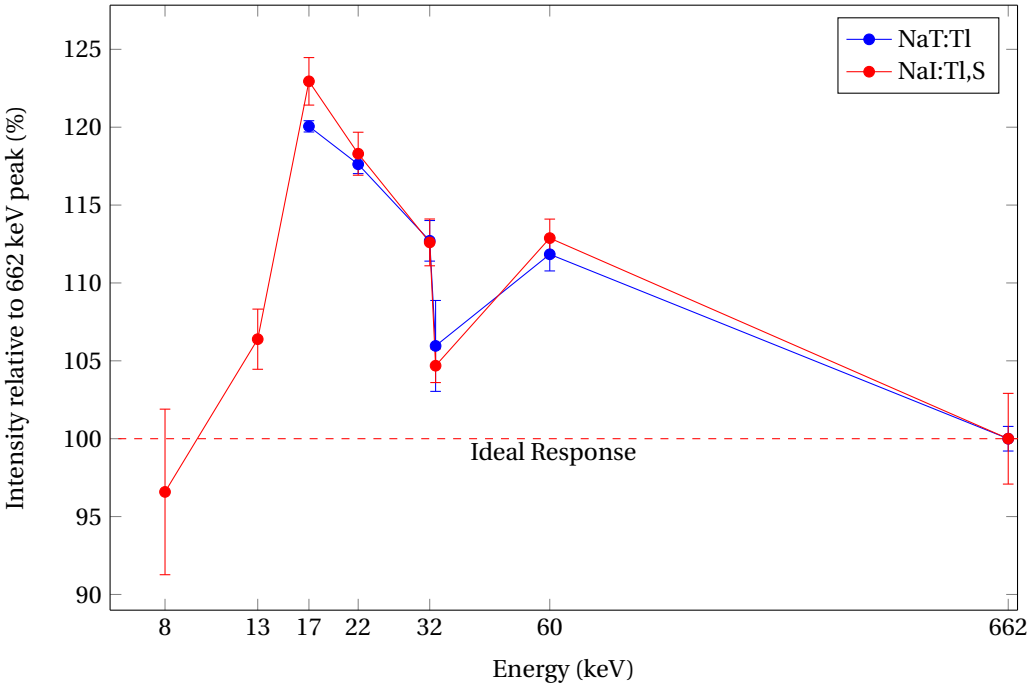


**Figure 4.5:** *Non-proportionality response relative to the 662 keV peak intensity of NaI:Tl and NaI:Tl,S at room temperature.*

The resolution of both crystals are presented in Table 4.3.

**Table 4.3:** *Resolution of bare NaI:Tl and NaI:Tl,S crystals at room temperature.*

| Crystal | Resolution (%) | light yield (phe/$keV$) at 662 keV | $R_M$ (%) |
|---|---|---|---|
| NaI:Tl | $6.0 \pm 0.3$ | $27 \pm 0.6$ | 2.0 |
| NaI:Tl,S | $11.4 \pm 0.7$ | $8.6 \pm 0.5$ | 3.6 |

The resolution of the sulphur doped crystal is significantly higher than that of the crystal doped with only thallium. Also the light yield of the NaI:Tl,S crystal is much lower than that of NaI:Tl. The lower light yield could be the result of the black dots present inside of the crystal; see Section 3.1.1. Equation (2.12) was used to determine the contribution of the PMT to the resolution ($R_M$) and this contribution is specified in Table 4.3. From these results it is shown that $R_M$ does not account for the large difference in resolution. Also from Figure 4.5 it is evident that the non-proportionality response does not differ greatly either. Therefore, the large difference in resolution can be attributed to either the transition resolution or the inhomogeneity of the crystal, according to Equation (2.11).

### 4.3.3. Co-doped $CeBr_3$ crystals

The non-proportionality of $CeBr_3$ crystals co-doped with Cd, Y, Lu, Sr and Na, and Sr and Ca, respectively, was determined as shown in Figure 4.6. The pulse height measurements were performed at room temperature, while the crystals were irradiated with Cs-137, Am-241 and the variable X-ray source; see Section 3.3.2 for details.

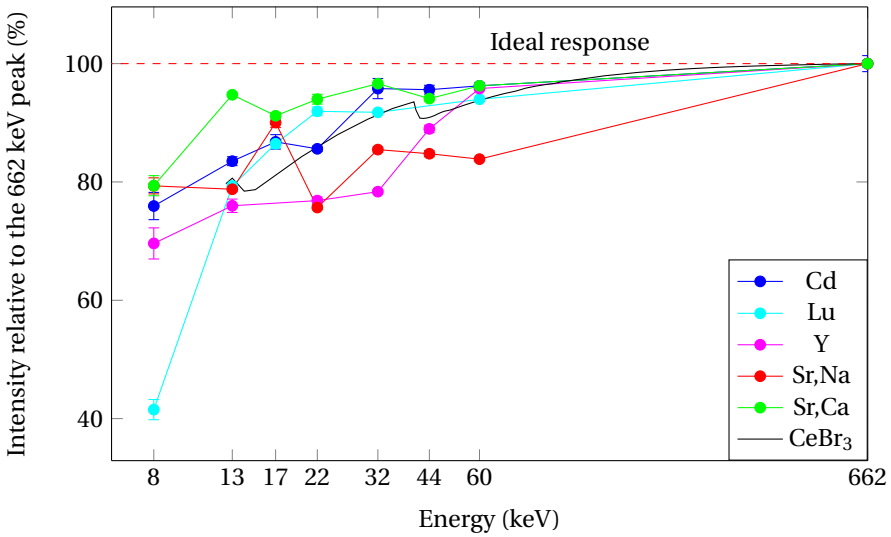


**Figure 4.6:** *Non-proportionality response of the $CeBr_3$ co-dopant crystals at room temperature relative to the 662 keV peak.*

Figure 4.6 shows that $CeBr_3$:Cd and $CeBr_3$:Sr,Ca have a more proportional response than undoped $CeBr_3$. All these crystals have divalent cations. $CeBr_3$:Lu looks promising, however, it has a very poor proportionality at 8 keV. $CeBr_3$:Y has a less proportional response compared with that of undoped $CeBr_3$. $CeBr_3$:Sr,Na shows a poor proportionality already at 60 keV and significantly under the response of undoped $CeBr_3$. At energies below 17 keV, however, the proportionality response of $CeBr_3$:Sr,Na is better than that of $CeBr_3$. At energies 17 keV and 8 keV the response of $CeBr_3$:Sr,Na is the same as that of $CeBr_3$:Sr,Ca.

**Table 4.4:** *Resolution and light yield of the Co-doped $CeBr_3$ crystals at room temperature.*

| Crystal | Resolution (%) | Light yield (phe/keV) | $R_M$ (%) |
|---|---|---|---|
| $Cd^{2+}$ | $6.3 \pm 0.2$ | $15.4 \pm 0.4$ | 2.6 |
| $Y^{3+}$ | $6.4 \pm 0.1$ | $18.1 \pm 0.3$ | 2.4 |
| $Lu^{3+}$ | $5.1 \pm 0.1$ | $20 \pm 1$ | 2.3 |
| $Sr^{2+}$,$Ca^{2+}$ | $3.65 \pm 0.05$ | $19.9 \pm 0.4$ | 2.3 |
| $Sr^{2+}$,$Na^{+}$ | $5 \pm 1$ | $18.2 \pm 0.4$ | 2.4 |
| Undoped [23] | 3.9 | 20 | 2.1 |

The $CeBr_3$:Lu and $CeBr_3$:Sr,Ca has the highest light yield of the crystal series, see Table 4.4. The $CeBr_3$:Sr,Ca shows the best resolution of the co-doped crystals. This corresponds with the observation that $CeBr_3$:Sr,Ca has a more proportional response. $CeBr_3$:Cd has a low light yield and a low resolution. The low light yield indicates that this co-dopant suppresses the light yield at 662 keV to gain a more proportional response at lower energies. This light yield could be suppressed by deep traps. The low resolution could also be attributed to the small size of the crystal. It could also indicate inhomogeinity of the crystal because the co-dopant Cd may not be fully dissolved into the $CeBr_3$ crystal. $CeBr_3$:Y and $CeBr_3$:Lu have a similar light yield while $CeBr_3$:Lu has a better resolution, which corresponds with a more proportional response. $CeBr_3$:Sr,Na has a similar light yield as that of Sr,Ca, however, the resolution of Sr,Na is much greater than that of $CeBr_3$:Sr,Ca, corresponding with a less proportional response from $CeBr_3$:Sr,Na.

## 4.4. X-ray excited light pulse evolutions and decay constants

Light pulse evolutions were taken with the picosecond X-ray setup; see Section 4.3. From these evolutions the primary decay time constant of the scintillator crystals was determined in the temperature range from 77 K to 500 K. This primary decay time constant is the dominant decay time constant.

### 4.4.1. NaI:Tl and NaI:Tl,S Crystals

The decay evolution of both the NaI:Tl and NaI:Tl,S crystals show a distinct difference in response, for the temperature range 77 to 150 K and from 200 to 500 K; see Figures 4.7 – 4.12. In the low temperature range (77-150 K), the recorded pulse shape revealed,an undoped additional to the dominant decay component, also a fast decay component; see Figure 4.7. This fast decay component is not seen in the pulse recordings at higher temperatures (200-500 K); see Figure 4.11.

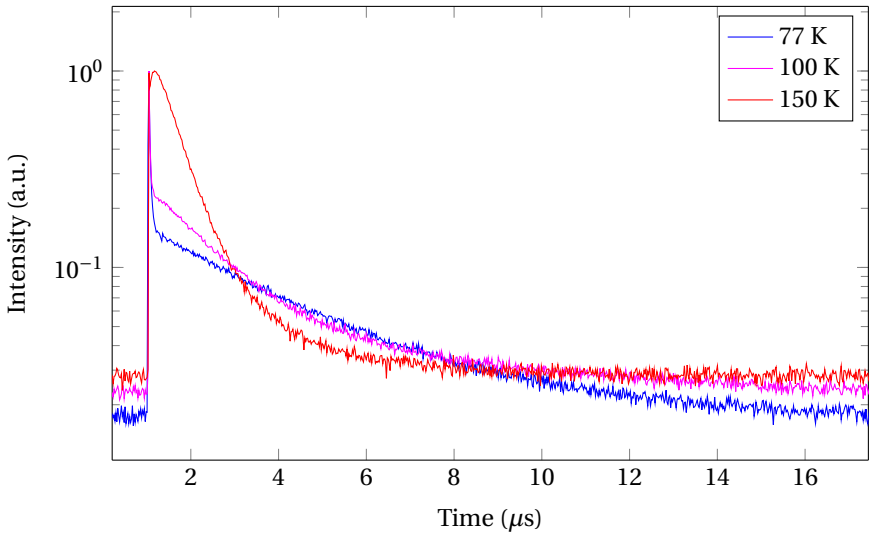


**Figure 4.7:** *Pulse shape of NaI:Tl crystal at 77, 100 and 150 K.*

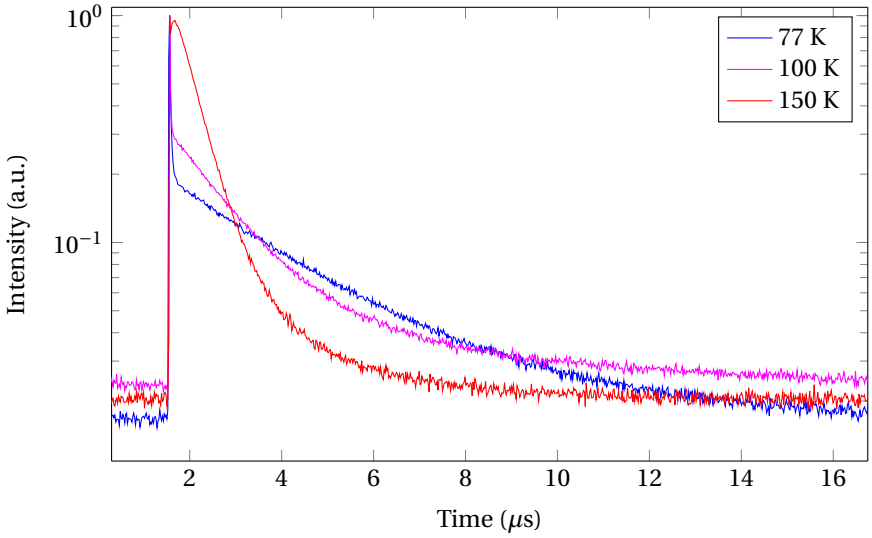


**Figure 4.8:** *Pulse shape of NaI:Tl,S crystal at 77, 100 and 150 K.*

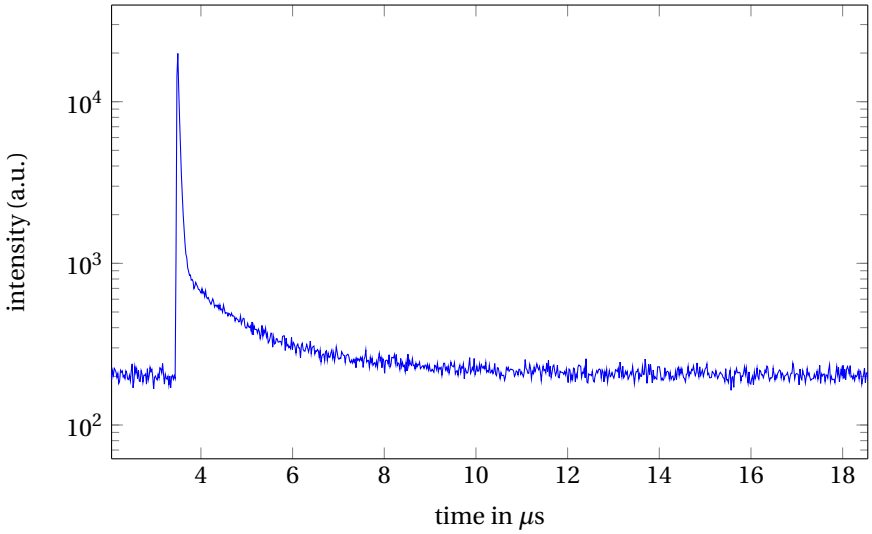


**Figure 4.9:** *Pulse shape of a undoped NaI crystal at 77 K.*

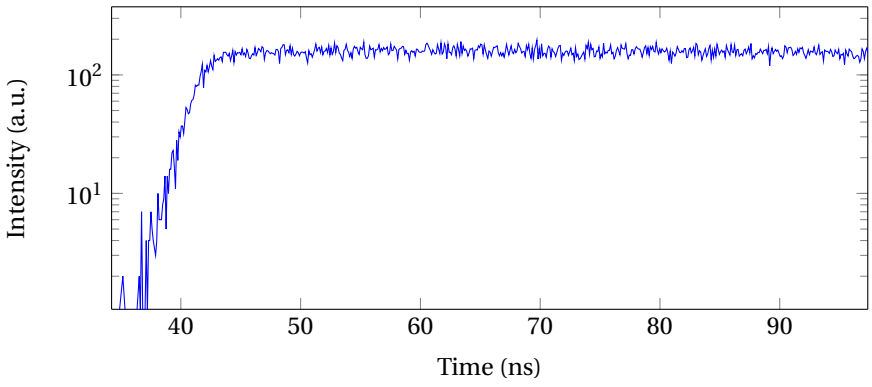


**Figure 4.10:** *Pulse shape of NaI:Tl crystal at 300 K measured with a small time window.*

The decay time constant of the fast component for NaI:Tl is 7 ns at 77, 100 and 150 K, respectively. This fast decay component is also observed in the light pulse evolution recorded from a undoped NaI crystal; see Figure 4.9. However, for undoped NaI the decay time was determined to be 25 ns at 77-150 K. This suggests that the decay process is associated with the NaI crystal and not with the $Tl^+$ dopant. This fast decay process may be associated with the low energy X-ray source (<40 $keV$) used in our experiment, since such a process was not observed when the crystal was excited with a high energy (662 keV). The fast decay process may become more likely with higher ionisation density, since the ionisation density increases with lower excitation energies; see Section 2.1.2. For higher temperatures (200-500 K) this fast component was not seen. This is due to a higher mobility at higher temperatures where the electrons are more likely to recombine via luminescent centres. However, this does not mean that the fast component completely disappears at temperatures above 200 K. Since the decay time decreases the height of the light peak attributed with the primary decay it may overlap the light peak attributed with the fast component. At temperatures above 150 K a flat top was observed; see Figure 4.10. This flat top could be attributed to the presence of the fast component as it overlaps the primairy decay process.

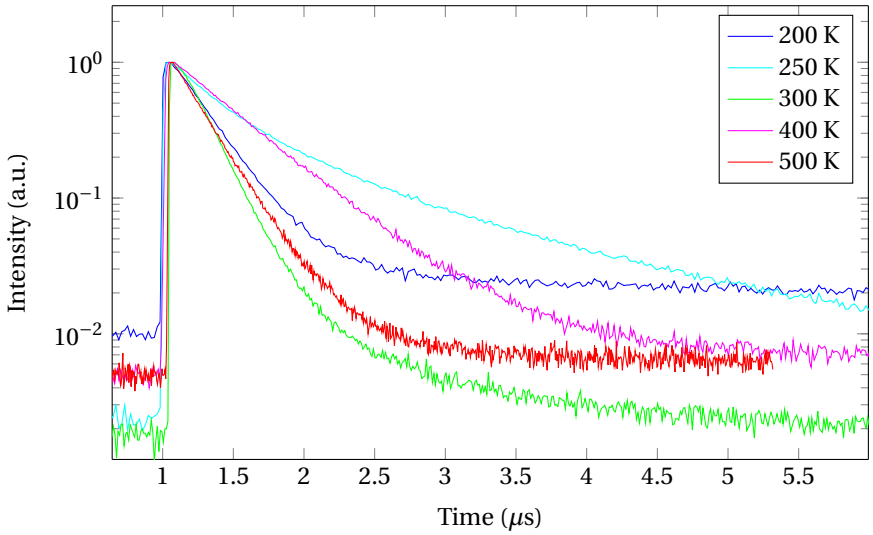


**Figure 4.11:** *Decay spectra of NaI:Tl crystal at 200-500 K.*

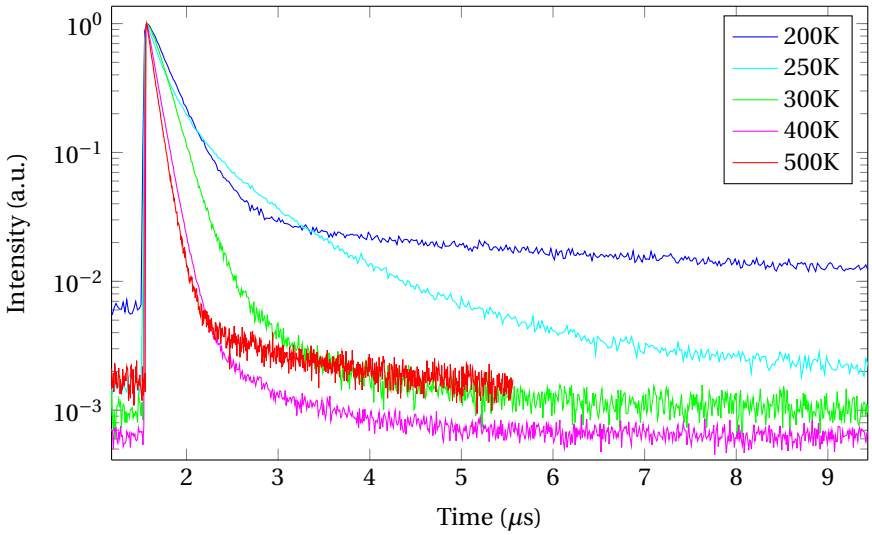


**Figure 4.12:** *Decay spectra of NaI:Tl,S crystal at 200-500 K.*

The decay time of the dominant light pulse component for both NaI:Tl and NaI:Tl,S crystals as a function of temperature is shown in Figure 4.13. The decay time constants of NaI:Tl and NaI:Tl,S crystals are very similar showing a exponentially decaying behaviour with temperature. Therefore, the difference in the transport resolutions would be little, as this resolution is related to the time elapsed untill they reach a luminescence takes place. This is as would be expected for $CeBr_3$ as the host crystal can luminece. This is due to increased mobility of the charge carriers towards luminescent centres at higher temperatures through diffusion; see Equation (2.7). The decay times determined here from the pulse shapes recorded with low energy X-rays (<40 $keV$) are shorter than the decay time constants determined from evolutions recorded with Cs-137 (662 keV) as reported in literature [1]. This is in agreement with the higher ionisation density when the light pulse evolutions are recorded at lower excitation energies, see Section 2.1.2.

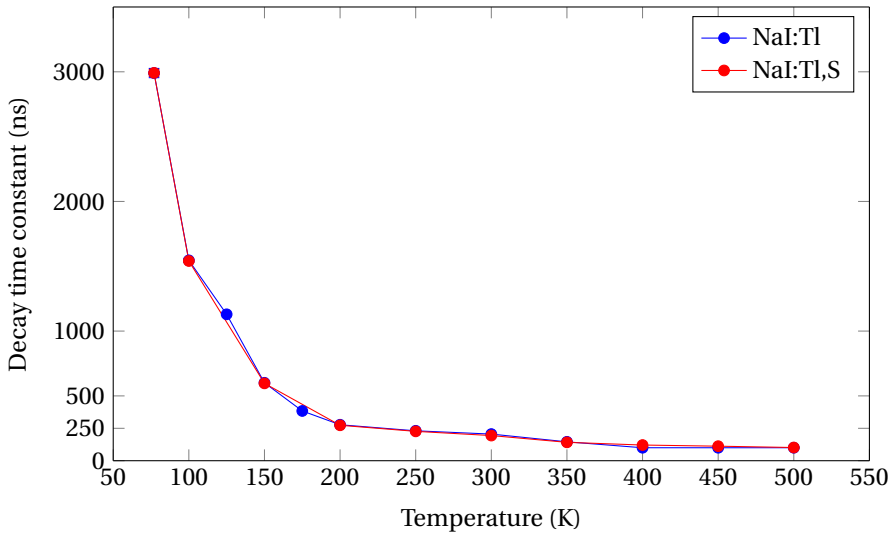


**Figure 4.13:** *Decay time constant versus temperature of the primary light pulse component of NaI:Tl and NaI:Tl,S crystals.*

### 4.4.2. Co-doped $CeBr_3$ crystals

In contrast with the NaI scintillator crystals, the co-doped $CeBr_3$ crystals show a small increase of the decay time with temperature; see Figure 4.14. Further, the decay times of the $CeBr_3$ crystals are 1 to 3 orders of magnitude shorter than those of the NaI crystals; compare with Figure 4.13. The short decay times and their weak dependence on temperature can be explained with the fact that $Ce^{3+}$ in the $CeBr_3$ crystal acts as a luminescent centre. Hence, the mobility of electrons towards the luminescent centres is less of a factor. The $CeBr_3$ crystals increase rather than decrease with increasing temperature. This is due to selfabsorption of $Ce^{3+}$ [12] since the process of emitting, re-absorbing and re-emitting logically increases decay time constant. Self absorption occurs when the intrinsic emission spectra overlaps the emission spectra of $Ce^{3+}$. Both emission spectra broaden as temperature increases, also increasing the chance of self-absorption.
All co-dopants cause a slower decay time constants than undoped $CeBr_3$, this is because of less luminescent centres due to the co-doping. The co-doped $CeBr_3$ crystal decay constants increase less as temperature increases than undoped $CeBr_3$ crystal. This indicates that the co-doped $CeBr_3$ crystals have a smaller chance of self-absorption than undoped $CeBr_3$. Interestingly, the decay time constant of the Cd co-doped $CeBr_3$ crystal at 500 K is lower than that of the undoped $CeBr_3$. As the dimensions of the crystal co-doped with Cd are the smallest (see Table 3.2) the chance of re-absorption of the luminescence before exiting the crystal is expected to be the smallest.
The decay time constants of the $CeBr_3$ crystals with isovalent co-dopants Y and Lu increases steadily with temperature; see Figure 4.14. Of the $CeBr_3$ crystal isovalent co-dopants Lu has the shortest decay time constant. This can be explained by the small dimensions of the Lu crystal; See Table 3.2. The divalent co-doped $CeBr_3$:Cd crystal has the smallest dimensions and increases the least as temperature rises, even having a smaller decay time constant at 500 K.
The double doped $CeBr_3$:Sr,Ca and $CeBr_3$:Sr,Na crystals show a different light pulse behaviour below 300 K. The decay time constants of $CeBr_3$:Sr,Ca decreases at temperatures below 150 K and steadily increases above 150 K. This can be due to the strong trapping of the $CeBr_3$:Sr,Ca crystal at low temperatures. The decay time constants of the $CeBr_3$:Sr,Na crystal increases and decreases very irregularly below 300 K; see Figure 4.14.

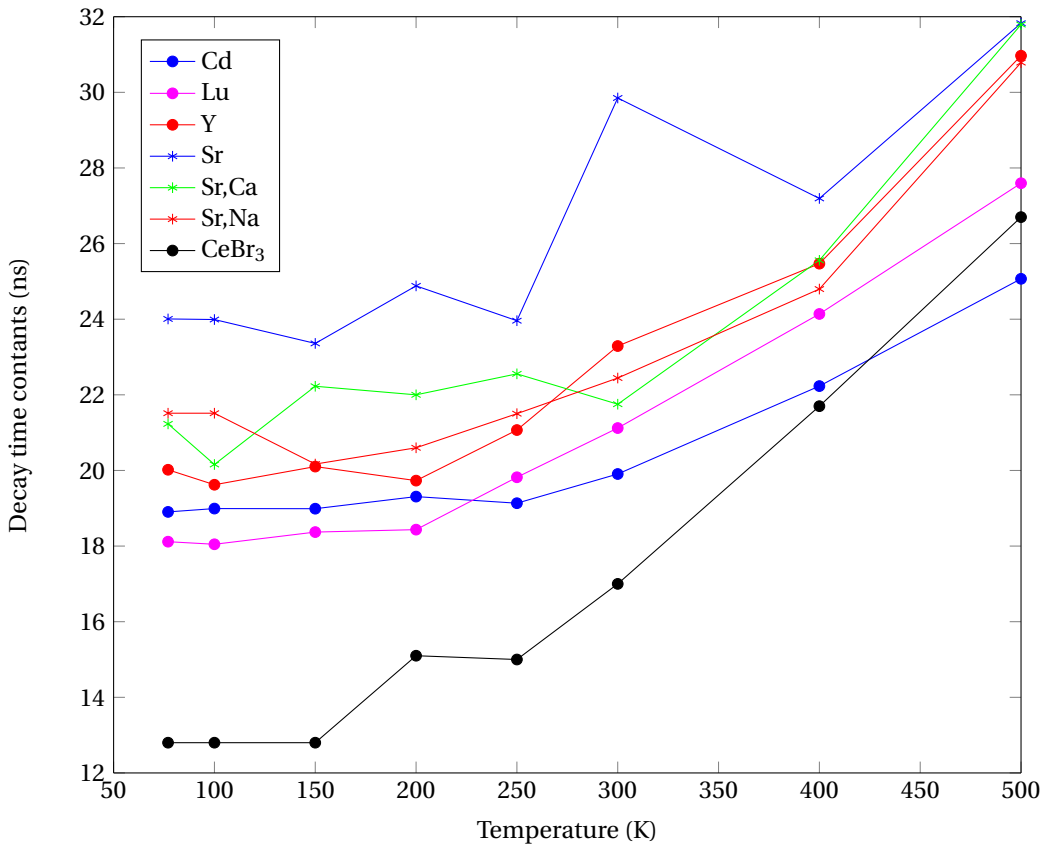


**Figure 4.14:** *Decay time versus temperature of $CeBr_3$ crystals with different co-dopants.*

## 4.5. Temperature Dependant Light Yield Measurements

The light yield of the doped and co-doped NaI and $CeBr_3$ crystals was measured using a Cs-137 source as a function of temperature in the range of 77 to 500 K; see Section 3.1. This light yield was determined with respect to the light yield observed at 300 K.

### 4.5.1. NaI:Tl and NaI:Tl,S Crystals

The light yield of the NaI:Tl and NaI:Tl,S crystals as a function of temperature is shown in Figure 4.15. For both crystals the highest light yield is observed at 250 K. At lower temperatures the light yield decreases due to a lower mobility of the electrons towards the luminescent centres in the crystal. The light yield of NaI:Tl,S does not increase as strongly as its thermoluminescence would suggest; compare with Figure 4.2. Remarkable is the dip of the light yield at 150 K for the NaI:Tl crystal; see Figure 4.15). Despite the strong trapping in the NaI:Tl crystal as suggested by the observed thermoluminescence (see Figure 4.2 the light yield below 150 K increases. This may be associated with the rise of the fast component in the light pulse decay evolution when going from 150 to 77 K; see Section 4.3.1 and Figure 4.7. The light yield of NaI:Tl,S, however, steadily decreases below 250 K. At temperatures above 250 K the light yield decreases due to quenching, i.e. the electrons lose energy to phonons; see Section 2.1.3. This quenching effect is stronger for the NaI:Tl compared with NaI:Tl,S crystal.

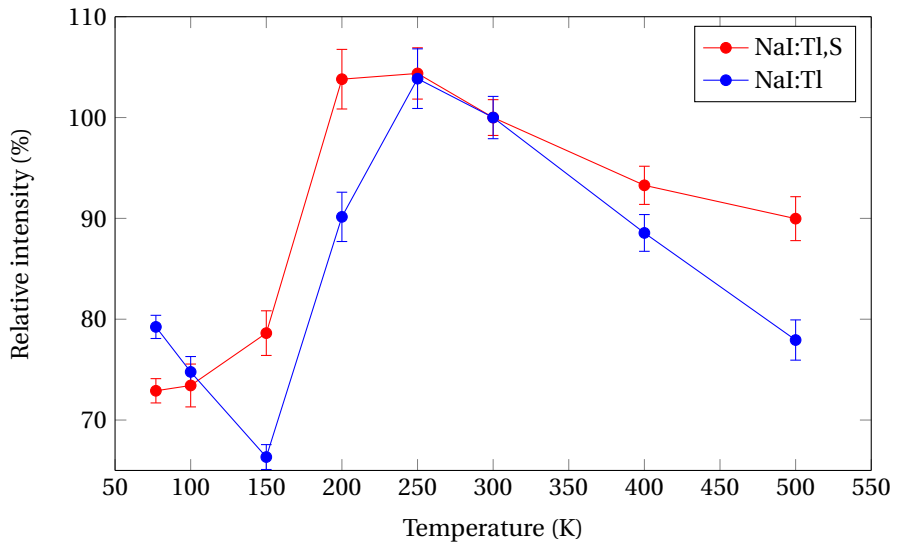


**Figure 4.15:** *Temperature dependence of the relative light yield of NaI:Tl and NaI:Tl,S crystals at 662 keV. The results were normalised to 100% at 300 K, which is the light yield at room temperature; see Table 4.3.*

### 4.5.2. Co-doped $CeBr_3$ Crystals

In contrast with the NaI crystals, $Ce^{3+}$ in the host $CeBr_3$ crystal acts as a luminescent centre; see Section 2.1.5. Therefore excited electrons are easily trapped by these luminescent centres. Thus the temperature dependant light yield of the co-doped $CeBr_3$ crystals is only dominated by quenching. The light yield of Sr,Ca doped $CeBr_3$ crystals decreases at temperatures below 250 K. This phenomenon is explained by the fact that as Sr,Ca co-dopants traps electrons before they can be trapped by the luminescent centres. This is supported by results from thermoluminescence measurements; see Section 4.1. Interesting is the increase of light yield of the $CeBr_3$:Cd crystal at temperatures below 200 K, which is significantly larger than that of undoped $CeBr_3$; see Figure 4.16. This indicates that the low light yield observed at room temperature improves more strongly at low temperatures. The quenching processes decrease in the $CeBr_3$:Cd crystal at lower temperatures. This indicates that when these charge carriers have less mobility they interact less with the co-dopant sites. This would indicate that the $Cd^{2+}$ sites decreases the luminescence of the crystal.

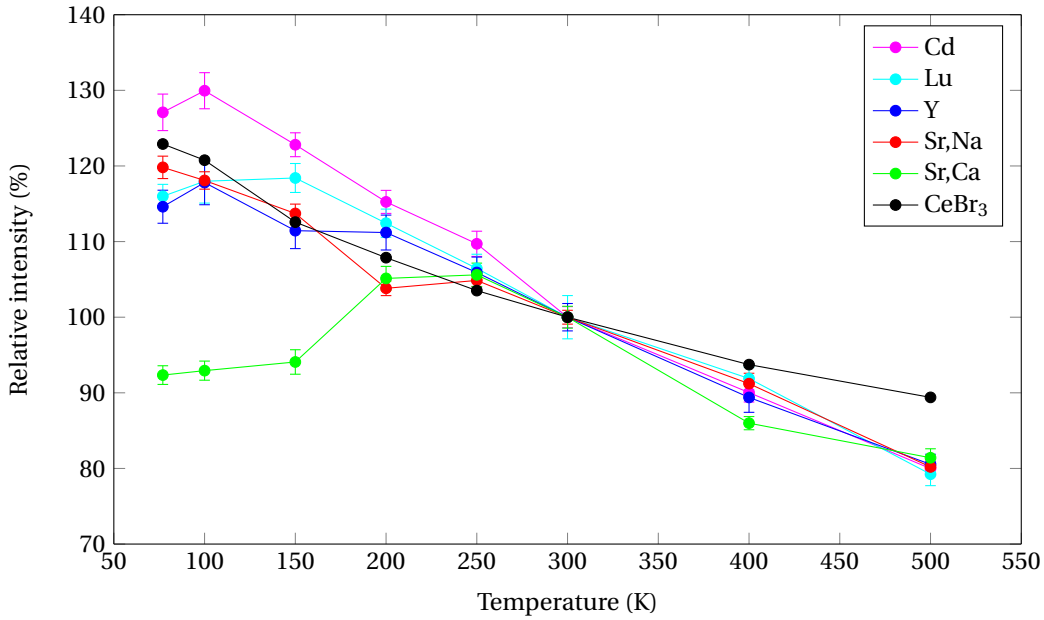


**Figure 4.16:** *Temperature dependence of the relative light yield of $CeBr_3$:Cd, $CeBr_3$:Sr, $CeBr_3$:Lu, $CeBr_3$:Y, $CeBr_3$:Sr,Na, $CeBr_3$:Ca,Sr and undoped $CeBr_3$ crystals at 662 keV. The results were normalised to 100% at 300 K, which is the light yield at room temperature; see Table 4.4.*

# 5

# Conclusions and recommendations

## 5.1. Conclusions

The properties determined of the NaI:Tl, NaI:Tl,S and NaI:Tl,Se scintillator crystals are governed by the quality of these crystals in terms of homogeneity of their composition and dissolution of the dopants into the crystals. The NaI:Tl,Se were black and no usable pulse height spectrum could be obtained. The NaI:Tl,S crystal also revealed inhomogeneity through its black dots. The NaI:Tl and NaI:Tl,S crystals showed similar luminescence spectra. Thus co-doping with sulphur does not act as a luminescence centre. The thermoluminescence of NaI:Tl,S suggests strong trapping of charge carriers by vancancies, which most likely originate from the crystal growth process. The co-doping with sulphur of the NaI:Tl crystal did not effect the shape of the non-proportionality curve. The light yield of NaI:Tl is much larger than that of NaI:Tl,S. Probably the light generated in the NaI:Tl,S crystal was absorbed by the black dots present. The inhomogeneous distribution of sulphur in the NaI:Tl,S crystal resulted in a lower resolution (11%) compared with that of NaI:Tl (6%). The thermoluminescence of the NaI:Tl,S crystal showed two more peaks compared with the thermoluminescence of the NaI:Tl crystal. Thus sulphur is not dissolved into the crystal lattice and probably all sulphur is concentrated at the observed black dots. It is noted that the NaI:Tl,S and the NaI:Tl,Se crystals were both grown at Bern university, and this was their first attempt growing such crystals.

Interestingly, a strong fast component is observed in the light intensity decay evolution of the NaI:Tl crystal for low temperatures, while excited with low energy X-rays (< keV). This fast component could be related to its non-proportionality response. The light yield of both NaI:Tl and NaI:Tl,S crystals is at maximum at 250 K, but the light yield of the NaI:Tl,S crystal is less temperature dependent. The light yield of NaI:Tl crystal is at minimum at 150 K and increases when going to 77 K. This is explained with the rise of the fast component of the light intensity decay.

The $CeBr_3$ with isovalent co-dopants (Y, Lu), showed perturbation of the $Ce^{3+}$ photoelectron doublet and light traps where this was not expected. The perturbation and the light traps are caused by defects not associated with the co-dopants. Therefore, it is questionable whether Y and Lu are fully dissolved into the crystal lattice. The improvement of the light yield at low temperatures is stronger for the $CeBr_3$:Lu crystal compared with that of the undoped and the Y co-doped $CeBr_3$ crystals, suggesting that Lu is better dissolved

than Y into the $CeBr_3$ crystal lattice. The divalent co-dopant Cd results in a strong perturbation of the $Ce^{3+}$ photoelectron doublet and so-called deep traps in the $CeBr_3$ crystal. This causes a weak thermoluminescence intensity as well as low light yield, which strongly improves with decreasing temperature. The double co-doped $CeBr_3$:Sr,Ca crystal showed the strongest perturbation of the $Ce^{3+}$ photoelectron doublet and highest thermoluminescence below 200 K. This is reflected by the decrease of the light yield in the temperature range of 77 to 200 K. Thus the double dopants Sr,Ca results in a high trapping density. Compared with Sr,Ca as co-dopants, Sr,Na shows a weak perturbation of the $Ce^{3+}$ doublet. The single valent Na co-dopant in combination with the divalent Sr, causes a low trapping probability for electrons. This is supported by the observed weak thermoluminescence.

Out of the $CeBr_3$ crystals with different co-dopants, the crystal with Sr,Ca displays the most proportional behaviour and the highest resolution as well as light yield. The crystal with Sr,Na as co-dopants, on the contrary, has a low resolution and low light yield. The isolvalent co-dopants Y and Lu both show a moderate proportional behaviour and a low resolution, but Y results in a low whereas Lu in a high light yield (similar as Sr,Ca). The co-dopant Lu shows an anomaly at 8 keV in the non-proportionality response curve (proportionality equals 40%). Cd as a co-dopant displays the lowest light yield and a low resolution, but a reasonable proportionality. The low resolution for all co-dopants except for Sr,Ca are likely caused by inhomogeneity of the crystals.

## 5.2. Recommendations

*Growth of the crystals*

It is expected that $CeBr_3$ co-doped with isovalent ions should deliver less self-absorption of the $CeBr_3$ crystal. However, this was not fully observed in this research. Therefore, the growth of $CeBr_3$ crystal with Y and Lu as co-dopant should be investigated to improve the dissolution of the co-dopants into the crystal lattice and to minimise defects.
As this was the first attempt at University of Bern to grow NaI crystals, it would be prudent to grow the NaI:TL,Se and NaI:Tl,S a second time, before discarding these co-dopants. If the second attempt yields clear crystals they would still be worth investigating.

*Quality of the scintillator crystals*

Based on the results obtained for the properties of the different scintillator crystals, it is recommended to have better control over the growth process of the crystals. Yet, the actual composition with regard to the amount of dopant and purity is unknown. Also the results suggests that the (co-)dopants may not have been fully dissolved into the crystal lattice. To study the effects of (co-)dopants on the scintillator performance, it is paramount to characterise the crystal composition as well as the dissolution of the co-dopant. Therefore analyses of the crystals using dedicated techniques prior to determination of their scintillation properties is advised.

*Fast X-ray excited light decay component*

The fast decay component observed in the light intensity decay of the NaI:Tl crystals should be studied in more detail, since this feature may effect the non-proportionality behaviour of these scintillator crystals. Knowledge of the nature of the fast decay may give directions to improve the proportionality of the scintillator material.

Experimental set-up
The experience gained during the execution of the experiments led to the following recommendations:

- When controlling the temperature of the crystal inside the cryostat it appeared that the temperature reading differs from the actual temperature, e.g. at liquid Nitrogen the temperature reading was about 1 to 6 K off. It is therefore advised to calibrate the temperature measurement over the whole temperature range of 77-500 K.
- When using the strong radioactive Cs-137 source, the yield of X-rays at 32 keV was so low that it could not be observed. This is due to absorption by the stainless steel container. It is therefore advised to use another container material with a low absorption for X-rays, e.g. aluminium. Also inside the cryostat, where the scintillator crystal is located, absorption of X-rays is of concern. Therefore the material between the X-ray source and the scintillator crystal to be investigated should have a low absorption, e.g. beryllium.

# A

# Appendices

## A.1. Counting Statistics

Radioactive decay is a random process. Consequently, any measurement taken from a radioactive process is subject to statistical fluctuation. Because the scintillator detector output gives a number of 'counts' inside a voltage range. For this thesis we are interested in finding peaks. That is a more than average amount of counts in a certain area. The following sections contains information about the way the peaks are expected to be distributed.

### A.1.1. Poisson Distribution

The Poisson process is a simple kind of random process, which models the occurrence of random points in a certain variable [24]. In order to justify the use of the Poisson distribution, two assumptions must hold:

1. The rate $\lambda$ is constant over time. (Homogeneity)
2. The number of arrivals in disjoint intervals are independent random variables. (Independence)

In terms of radioactivity this means that the half/life of the isotope does not change during the acquisition and that the decay events occur statistically independent of each other. This holds for radioactive isotopes used in this study.

This translates for the scintillator to the number of photons arriving on the photo cathode within a short time interval. The expected number of photons arriving for a given decay event is constant (unless it is the $\beta$ continuum) and number of arriving photons can be seen as independent random variables. It can therefore be assumed that the peaks discovered by the scintillator are Poissonian distributed.
When the number of photons is sufficiently high (higher than 20) the peak caused by the poisson distribution can be reliably approximated by a Gaussian distribution. [2]

### A.1.2. Gaussian Distribution

The simplification of the Poisson distribution leads to the following normalised Gaussian distribution [2]:

$$P(x) = \frac{1}{\sqrt{2\pi\bar{x}}} \exp\left(-\frac{(x-\bar{x})^2}{2\bar{x}}\right) \tag{A.1}$$

As is shown in Equation (A.1) the distribution is characterised by a single parameter $\bar{x}$. Both the mean value as the variance is equal to $\bar{x}$ as with the Poisson distribution.

The $\bar{x}$ is the position of the peak where the events of the radioactive decay is counted. In reality the variance of the peak is also determined by the resolution of the scintillator detector used.

## A.2. Peakfit

To determine the peak position and full width at half maximum, the pulse height spectrum was analysed in MATLAB using Gaussian fits. An example of such a fit is presented in A.1.

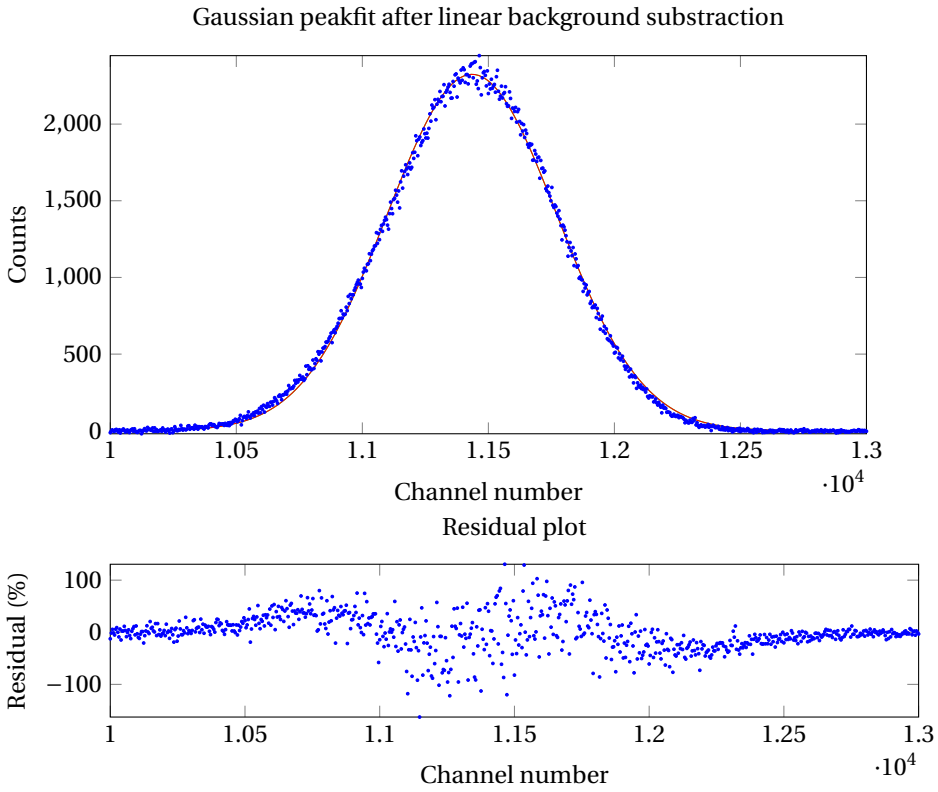


**Figure A.1:** A Gaussian fitting to the experimental data.

When different peaks overlap an equal width Gaussian fit was used to identify these peaks.

## Acknowledgements

First of all, I thank my supervisors professor Pieter Dorenbos and Roy Awater (MSc) for their stimulating discussions, excellent guidance and critical reading of this thesis and I am also grateful for their valuable suggestions.

I am thankful to Johan de Haas who provided indispensable technical support during my experimentation.

Finally, I express my gratitude to my family and friends for their support and keeping faith in me.

# Bibliography


[1] P. A. Rodnyi. *Physical Processes in Inorganic Scintillator Crystals*, chapter 1.1, pages 1–9. CRC Press, New York, 1997.

[2] G. F. Knoll. *Radiation Detection and measurements*, chapter 2. John Wiley and Sons, inc, 1999.

[3] F.G.A. Quarati. *$LaBr_3$ gamma-ray spectrometers for space exploration*. PhD thesis, Delft University of Technology, 2013.

[4] M. Alekhin. *New halide scintillators for gamma ray detection*. PhD thesis, Delft University of Technology, 2013.

[5] R. Hofstadter. *Phys Rev 75*, 1949.

[6] J.T.M. de Haas P. Dorenbos and C.W.E. van Eijk. Non-proportionality in the scintillator response and the energy resolution obtainable with scintillator crystals. *IEEE Transactions on Nuclear Science*, 1995.

[7] W.W.W. Drosdowski; P. Dorenbos; A.J.J. Bos; G. Bizarri; A. Owens; F.G.A. Quarati. *$CeBr_3$ scintillator development for possible use in space missions*. IEEE Transations on Nuclear Science, 2008.

[8] J. Buzniak K. Y. Jan and Vladimir Ouspenski. Performance Improvement of Large Sr2+ and Ba2+ co-doped LaBr3:Ce3+ Scintillation Crystals. *IEEE Nuclear Science Symposiwn and Medical Imaging Conference Record (NSS/MIC)*, 2012.

[9] W. W. Moses; G. A. Bizarri; R. T. Williams; S. A. Payne; A. N. Vasilev; J. Singh; J. Q. Grim and W. S. Choong. The orinigins of scintillator non-proportionality. *IEEE Transactions on Nuclear Science*, 2012.

[10] Ivan Khodyuk. *Nonproportionality of inorganic scintillators*. PhD thesis, Delft University of Technology, 2013.

[11] C Pedrini. Scintillation mechanisms and limiting factors on each step of relaxation of elelectron excitations. *Phys. Solid State*, 2005.

[12] Dennis R. Schaart D. N. ter Weele and P. Dorenbos. The Effect of Self-Absorption on Scintillation properties of $Ce^{3+}$ Activated $LaBr_3$ and $CeBr_3$. *IEEE Transactions on Nuclear Science*, 2014.

[13] Saint Gobain NaI:Tl data sheet. `http://www.crystals.saint-gobain.com/uploadedFiles/SG-Crystals/Documents/NaI(Tl)%20Data%20Sheet.pdf`. Accessed: 2016-07-10.

[14] Henderson and G.F. Imbusch. *Optical Spectroscopy of Inorganic Solids*. Oxford University Press, 1989.

[15] D. Brown. *Halides of the Transition Elements: Halides of the Lanthanides and Actinides*, chapter 5. Wiley, 1968.

[16] Mark J. Harrison; Christopher Linnick; Benjamin Montag; Samuel Brinton; Mark McCreary; F. P. Doty; and Douglas S. McGregor. Scintillation performance of aliovalently-doped cebr3. *Nuclear Intruments and Methods in Physics Research A)*, 2013.

[17] D. R. Lide. *CRC Handbook of Chemistry and Physics*, pages 201–213. CRC Press, 2005.

[18] Richard J.D. Tilley. *Defects in solids*, chapter 3.8, pages 103–105. Wiley, 2008.

[19] P. Dorenbos. $Ce^{3+}$ 5d-centroid shift and vacuum referred 4f electron binding energies of all lanthide impurities in 150 different compounds. *Journal of Luminescence*, 2013.

[20] P. Dorenbos J.T.M.De Haas. Methods for accurate measurement of the response of photomultiplier tubes and intensity of light pulses. *IEEE Transactions on Nuclear Science*, 2010.

[21] Hamatsu PMT handbook chapter 4. `https://www.hamamatsu.com/resources/pdf/etd/PMT_handbook_v3aE-Chapter4.pdf`. Accessed: 2016-07-10.

[22] K.W. Kramer; P. Dorenbos F.G.A. Quarati, M.S. Alekhin. Co-doping of CeBr3 scintillator detectors for energy resolution enhancement. *Nuclear Intruments and Methods in Physics Research A)*, 2013.

[23] F.G.A. Quarati; M.S. Alekhin; K.W. Kramer; P. Dorenbos. Co-doping of $CeBr_3$ scintillator detectors for energy resolution enhancement. *Nuclear Instruments and Metheds in Physics Research A*, 2013.

[24] F.M. Dekker; C. Kraaikamp; H.P. Lopuhaa; L.E. Meester. *A Modern Introduction to Probability and Statistics*, pages 170–171. Springer, 2005.